FULL PAPER

Eight-year catalog of deep short-term slow slip events at the Nankai trough based on objective detection algorithm using strain and tilt records

Suguru Yabe[1*] , Tadafumi Ochi[1], Norio Matsumoto[1], Satoshi Itaba[1], Yuichi Kitagawa[1] and Takanori Matsuzawa[2]

Abstract

In subduction zones, slip deficit monitoring along the plate interface is important for understanding the seismogenesis of megathrust earthquakes. In the last two decades, aseismic slip transients, such as slow slip events (SSEs), which are usually synchronized with tectonic tremors, have been detected in subduction zones worldwide. Frequent SSEs are particularly important for releasing slip deficits during the inter-seismic periods of megathrust earthquakes. In southwest Japan, deep short-term SSEs have been primarily monitored with strain and tilt records because the SSEs in this region are small. However, strain and tilt records are so sensitive that they record not only SSEs, but also rainfall and local groundwater movements, which temporally affect the quality of data making it difficult to apply an automated detection algorithm. Therefore, previously reported short-term SSE catalogs, based on strain and tilt records, were created by visual inspections, although they are not suitable for generating a long-term catalog. In this study, a quantitative detection algorithm was developed to detect short-term SSEs using strain and tilt records. The problem of temporally varying data quality was solved by introducing the prior probability of log-normal distributions in the fitting variance. This method was applied to an 8-year (2013–2020) dataset of strains and tilts from southwest Japan. A total of 96 events were detected, among which, 78 corresponded with SSEs previously reported by the Geological Survey of Japan (GSJ). Although the GSJ catalog contained more events with smaller magnitudes, such events were difficult to distinguish from noise using the developed method. Three of the remaining 18 events were considered SSEs that were not reported in the GSJ catalog. Others could be artifacts because there were no obvious signals in the global navigation satellite system records (with events of magnitude > 6.0). Previous studies have suggested the existence of aseismic transients deeper or shallower than regular short-term SSEs in southwest Japan. However, detection results from this study did not confirm such events.

Keywords Strain, Tilt, Slow earthquake, Slow slip events, Southwest Japan, Nankai trough, Objective detection
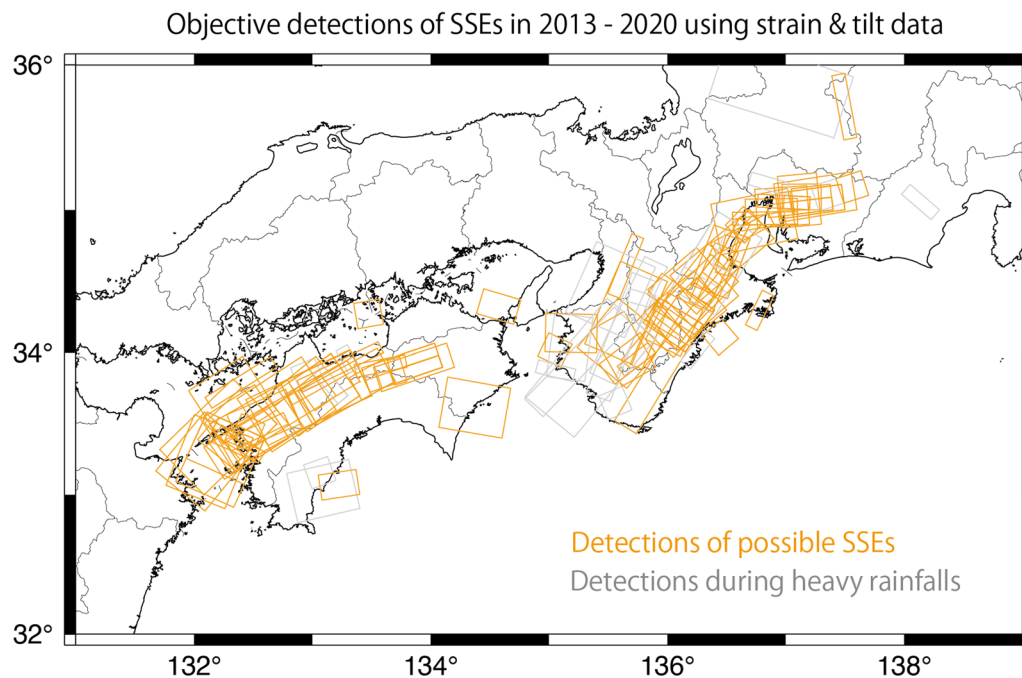
*Correspondence:
Suguru Yabe
s.yabe@aist.go.jp
Full list of author information is available at the end of the article

---

Graphical Abstract

Objective detections of SSEs in 2013 - 2020 using strain & tilt data

Detections of possible SSEs
Detections during heavy rainfalls

Introduction

In subduction zones, megathrust earthquakes have been repeatedly occurring, causing disasters in society (Ando 1975; Ammon et al. 2005; Ide et al. 2011). They release strain which has been accumulated through plate subduction. Monitoring slip deficit accumulation in subduction zones is crucial, and there are many previous studies on this (e.g., Yoshioka and Matsuoka 2013; Loveless and Meade 2016; Yokota et al. 2016; Noda et al. 2018). The accumulated strain is released through seismic ruptures as well as through aseismic phenomena (Ozawa et al. 2001; Wallace and Beavan 2010; Villegas-Lanza et al. 2016). One of the important aseismic phenomena is "slow earthquake". Slow earthquakes were discovered at the beginning of the twenty-first century in southwest Japan and Cascadia (Dragert et al. 2001; Obara 2002). Seismic and geodetic signals of slow earthquakes are termed differently: low frequency earthquakes (LFEs) or tectonic tremors in 2–8 Hz (Obara 2002); very low frequency earthquakes in 0.005–0.05 Hz (Ito et al. 2007), and slow slip events (SSEs) in the geodetic range (Hirose et al. 1999; Dragert et al. 2001). These signals are often temporary and spatially correlated (Rogers and Dragert 2003; Obara et al. 2004) and are considered to represent narrow-band signatures of broadband slow earthquakes (Kaneko

et al. 2018; Ide & Yabe 2019; Masuda et al. 2020). That is, high LFE or tremor activities imply large seismic moment release in accompanying SSEs (Maeda and Obara 2009; Frank et al. 2018). In subduction zones, focal mechanisms of tectonic tremors, very low frequency earthquakes, and SSEs are estimated to be low-angle thrusts, consistent with subducting plate interface (Ide et al. 2007a; Ito et al. 2007; Ide & Yabe 2014). However, slow earthquakes have a longer duration than regular earthquakes with the same moment (Ide et al. 2007b). Slow earthquakes have been detected globally in various tectonic settings (Behr and Burgmann 2021), such as subduction zones (Wallace and Beavan 2010; Radiguet et al. 2012), collision zones (Liu et al. 2009), transform faults (Nadeau and Dolenc 2005; Wech et al. 2012), and inland faults (Chao and Obara 2016). Slow earthquakes may play an important role in the nucleation process of large earthquakes (Ando and Imanishi 2011; Kato et al. 2012; Ruiz et al. 2014; Yabe and Ide 2018), and slow earthquakes studies have been conducted worldwide.

In this study, the study area is southwest Japan, where short-term SSEs are difficult to monitor owing to their small sizes. Here, slow earthquake zones and locked zones for the anticipated megathrust earthquakes are distributed separately in depth (Obara and Kato 2016). In

Yabe *et al. Earth, Planets and Space*   (2023) 75:13

Page 3 of 21

the Nankai subduction zone, deep short-term SSEs and tremors are located at 30–40 km depths, referred to as "regular SSE regions" in this study, and the plate interface is locked at shallow depth. The maximum magnitude of deep short-term SSEs is less than 6.5 (Sekine et al. 2010; Hirose et al. 2020). Such small signals were difficult to be detected using global navigation satellite system records (GNSS) during the early stages of slow earthquake studies in southwest Japan, unlike in Cascadia, where short-term SSEs with magnitude greater than 6.5 often occur (Szeliga et al. 2008). Instead, tiltmeters, which were deployed in the seismic network by the National Research Institute for Earth Science and Disaster Resilience (NIED), were used to detect short-term SSE signals (Obara et al. 2004). Tilt (i.e., spatial gradients of displacement) is sensitive enough to detect small SSE signals. A rectangular single fault was usually assumed for estimating the fault models of SSEs to reveal temporal and spatial synchronization of tremors and SSEs as well as along-strike variations of slow earthquake activities (Obara et al. 2004; Hirose and Obara 2006; Sekine et al. 2010). Recently, detailed slip distributions of short-term SSEs were estimated using tilt records, by dividing the faults into smaller sub-faults (Hirose and Kimura 2020a, b). The minimum magnitude of SSEs, detected using tilt records, was 5.7 (Sekine et al. 2010; Hirose and Kimura 2020a, b). However, many tectonic tremor activities have been reported when any SSEs were not reported from the tilt records (Hirose & Kimura 2020a, b). Considering the spatial and temporal synchronization of tremors and SSEs, small SSEs, which are difficult to be detected with tilt records, are expected to occur during these times.

The Geological Survey of Japan (GSJ), National Institute of Advanced Industrial Science and Technology constructed a strain observation network in southwest Japan for the purpose of improving the short-term SSE detection (Itaba et al. 2010). The Japan Meteorological Agency (JMA) also constructed a strain observation network in the Tokai region (Suyehiro 1979; Furuya and Fukudome. 1986; Miyaoka and Yokota 2012; JMA 2022a, b). Although the original purpose of JMA strain network was to detect preslip of the anticipated Tokai earthquake, they are now used for SSE monitoring. SSE monitoring by GSJ is conducted using observation data from GSJ, JMA, and NIED and are reported monthly to governmental committees as well as the Coordinating Committee for Earthquake Prediction, Japan (CCEP-J). According to the short-term SSE catalog of GSJ in the CCEP-J reports, the minimum magnitude of SSE was 5.2, which is lower than detections using only tilt records (Itaba et al. 2013, 2014a, 2014b, 2015; Ochi et al. 2015, 2016a, 2016b, 2017a, 2017b, 2018a, 2018b, 2019a, 2019b; Yabe et al. 2020a, 2020b, 2021a, 2021b).

Short-term SSE signals are now detectable in GNSS records by applying a geodetic-matched filter technique (Nishimura et al. 2013; Nishimura 2014). Using a duration of 180 days, a linear function is fitted to the GNSS data along the dip direction, with and without an offset in the middle of the duration. Akaike's Information Criteria (AIC) are calculated for the two models to determine which model fits the observed data better. When the former model is found to be superior, the estimated offset value is considered to be the amount of deformation caused by the SSEs. Differences in AICs between the two models are stacked for nearby stations and used for SSE detection with quantitative criteria. Okada et al. (2022) modified the methodology to include duration information in the estimated source parameters. Kano et al. (2019) and Kano and Kato (2020) used different approaches to study short-term SSEs using GNSS data. As it is difficult to obtain detailed slip distributions of individual events using GNSS records, GNSS data are stacked during periods when tectonic tremors are active, and slip distributions of stacked SSEs are estimated. Consequently, the slip invading the shallow locked zone was estimated, in addition to the large slips in regular SSE regions.

In the GSJ catalog, short-term SSE detections or their periods were determined by visual inspection (Itaba et al. 2013), similar to the analysis of the NIED tilt data (Hirose et al. 2020). An automated detection algorithm for strain and tilt data was difficult because of data quality. These data were sufficiently sensitive to detect small SSE signals. However, they are so sensitive that they capture signals from non-tectonic causes as well, such as local deformation caused by rainfall and groundwater movement (e.g., Jahr 2018; Canitano et al. 2021). Therefore, the quality of strain and tilt data for SSE detection is variable not only among stations, but also temporally. However, similar to the GNSS data, quantitative detection is needed to construct a uniform short-term SSE catalog for the region (Nishimura et al. 2013; Nishimura 2014). If not, detection results may be influenced by differences in the subjective detection criteria (such as different analysts and/or different periods).

Kimura et al. (2011) constructed an automated short-term SSE detection algorithm with tilt data using the Kalman filter algorithm and grid search for estimating fault location, geometry, size, and slip direction of SSEs. Models with and without SSEs were compared and used for the detection of possible SSEs. Robustness tests were then conducted to remove false detections. The study detected four SSEs over 2 years in the Shikoku region, and ~400 false detections were removed during the robustness tests. A constant variance was assumed for noise in the model; subsequently, detection could be easily affected by temporally variable data quality.

Yabe *et al. Earth, Planets and Space*   (2023) 75:13

Page 4 of 21

This study proposes a method to estimate crustal deformations, possibly caused by slip on the plate interface, using strain and tilt data from the GSJ, JMA, and NIED. Problems due to the instabilities in data quality were solved by introducing prior distributions in the data fitting. Section "Data and preprocessing" explains the data used, preprocessing of data to remove tidal and barometric responses, and slow earthquake activities during the analysis period. In Section "Method", methodologies for automatically detecting the possible short-term SSEs from strain and tilt data and for estimating the final fault model for the detected events are provided. Section "Results and discussion" presents the detection results and a comparison with existing catalogs based on strain and tilt data and GNSS data. Additionally, the possibilities of shallow SSEs, as identified by Kano et al. (2019) and Kano and Kato (2020), based on stacked GNSS data, are discussed. Section "Conclusions" presents conclusions.

Data and preprocessing
Strain and tilt observations

This study used the strain and tilt data observed by GSJ, JMA, and NIED. The station distributions are shown in Fig. 1. The GSJ observation network consists of 17 stations located at regions from Tokai to Shikoku. Strainmeters and tiltmeters were deployed at each station. Two types of strainmeters were used in the network. Gladwin tensor strainmeters (GTSMs, Gladwin 1984) were deployed at four stations and Ishii-type strainmeters (Ishii et al. 2002; Asai et al. 2009) at the other stations. The data quality of GTSMs was poor compared with that of Ishii-type strainmeters; therefore, GTSM data were not used in this analysis. Ishii-type strainmeters measure the horizontal strain along the four azimuths. The data were converted to horizontal strain tensors by multiplying with the calibration matrices. Twenty-four stations from the observation networks in the JMA and Shizuoka Prefectures were used. Volumetric strainmeters were deployed at 13 stations. One set of Ishii-type strainmeters was deployed at five stations, and two sets
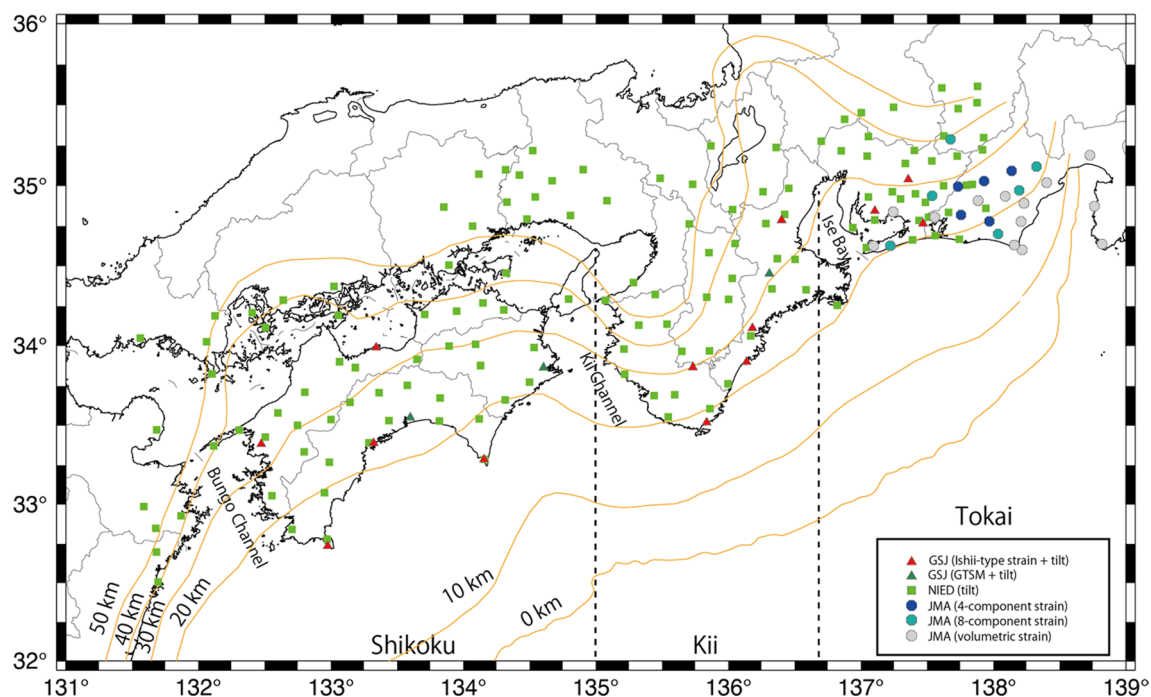

Fig. 1 Station map and tectonic settings of the southwest Japan. Red triangles are GSJ stations, where Ishii-type strainmeter and tiltmeters were deployed. Green triangles are GSJ stations, where Gladwin Tensor Strainmeter (GTSM) and tiltmeters were deployed. Green squares are NIED tiltmeters. Dark blue octagons are JMA stations, where one Ishii-type strainmeter is deployed. Light blue octagons are JMA stations, where two sets of Ishii-type strainmeters were deployed. Gray octagons are JMA stations, where volumetric strainmeters were deployed. Orange curves are the location of trench and iso-depth contours of subducting plate interface by Baba et al. (2002), Nakajima and Hasegawa (2007), and Hirose et al. (2008)

Yabe *et al. Earth, Planets and Space*   (2023) 75:13

Page 5 of 21

of Ishii-type strainmeters were deployed at six stations. Calibration coefficients (scalar) and matrices were multiplied by the observed volumetric and horizontal strain data during preprocessing, respectively. The NIED tiltmeters were collocated with Hi-net seismometers. The data used in this study were originally sampled at 20 Hz, and they were resampled with a sampling interval of one hour. Subsequently, the data were preprocessed. The study period was 2013 to 2020.

Preprocessing

Strain and tilt data contain not only crustal deformation due to tectonic events, but also local deformation due to tides, barometric pressure changes, rainfall, and groundwater movement. The BAYTAP-G program (Tamura et al. 1991) was used to remove the tidal and barometric responses from observations. BAYTAP-G assumes that crustal deformations are slow and can be represented by the Brownian motion. Based on this assumption, BAYTAP-G disassembled the observational data into trend terms, including signals of crustal deformations, tidal response terms, barometric response terms, and noise terms. The tidal response term was represented by the summation of sinusoidal curves with 15 tidal periods (diurnal and semidiurnal tides as well as M_3 tidal component as listed in Tamura et al. (1991)). The barometric response term was represented by the summation of instantaneous and time-delayed linear responses to barometric pressure changes. A time delay of up to three data points (3 h) was permitted. The time delay was determined by try and error. Barometric pressure changes were measured at the GSJ and JMA stations. For the NIED stations, the barometric pressure changes observed at the closest GSJ or JMA stations were used. As the noise term was assumed to follow a normal distribution, the disassembling of observation data was conducted based on least-square fitting.

Raw strain data are affected by material heterogeneity around the sensor, such as the cement used to hold the sensor in the borehole. Hence, the raw strain data must be calibrated for conducting the crustal deformation analysis. This study used the method described by Matsumoto et al. (2010) and Matsumoto and Kamigaichi (2021), where the calibration matrix or coefficient is estimated based on a comparison of observed and synthetic strains of M_2 and O_1 tidal constituents at each station (Hart et al. 1996; Roeloffs 2010). The ocean tidal loading effect of the synthetic strains was determined using Green's functions at the deployment depth of the borehole strainmeters (Kamigaichi et al. 2021).

For volumetric strain, the scalar calibration coefficients were multiplied by the raw values. For the horizontal strain, raw observation data along four horizontal azimuths were converted to a horizontal strain tensor. In this step, three components were selected from the four azimuth angles. The corresponding 3×3 calibration matrix was multiplied by the raw data to obtain the horizontal strain tensor. These calculations were done for all possible combinations of components, and the averages for the calibrated horizontal strain tensors were used.

Slow earthquake activity during 2013–2020

Slow earthquakes occurred repeatedly during the analysis period (Fig. 2). The LFE catalogs (Fig. 2a) were constructed by JMA and Kato and Nakagawa (2020). The number of events in the JMA catalog increased significantly from March 2018, owing to the changes in detection methodology. From this date, JMA started detecting LFEs using a matched filter technique (Shelly et al. 2007), in addition to the previous manual inspections conducted since 1999 (Nishide et al. 2000; Katsumata and Kamaya 2003; Nakamura 2006). Kato and Nakagawa (2020) constructed LFE catalogs prior to August 2015 using matched filter analysis. The short-term SSE catalogs were constructed by: (i) GSJ (Fig. 2b) (Itaba et al. 2013, 2014a, 2014b, 2015; Ochi et al. 2015, 2016a, 2016b, 2017a, 2017b, 2018a, 2018b, 2019a, 2019b; Yabe et al. 2020a, 2020b, 2021a, 2021b); (ii) NIED (Fig. 2c) (Kimura 2013, 2014, 2015a, 2015b, 2016a, 2016b, 2017a, 2017b, 2018a, 2018b, 2019a, 2019b, 2020a, 2020b, 2021; Kimura and Kimura 2014); (iii) Nishimura et al. (2013) and Nishimura (2014) (Fig. 2d). The SSE catalog of Hirose and Kimura (2020a, b) is based on the SSE catalog of the NIED. GSJ uses the strain and tilt data of GSJ, strain data of JMA, and tilt data of NIED, whereas NIED uses only tilt data of NIED, resulting in differences in the detected number of SSEs. Nishimura et al. (2013) detected SSEs using only GNSS data prior to 2013 in southwest Japan, and Nishimura (2014) detected SSEs using a method modified from Nishimura et al. (2013) in the Ryukyu Trench. The catalog presented here was analyzed using the method of Nishimura (2014) and updated up to 2020. Figure 2e shows the time plots of these catalogs for 2013–2020. Many SSEs were correlated with LFEs, though this has not been the case in the Ise-Bay region as noted by Obara and Sekine (2009). The timing of the SSEs detected by NIED coincides with those detected by the GSJ, whereas some SSEs detected by GNSS do not coincide with those detected by GSJ and NIED.
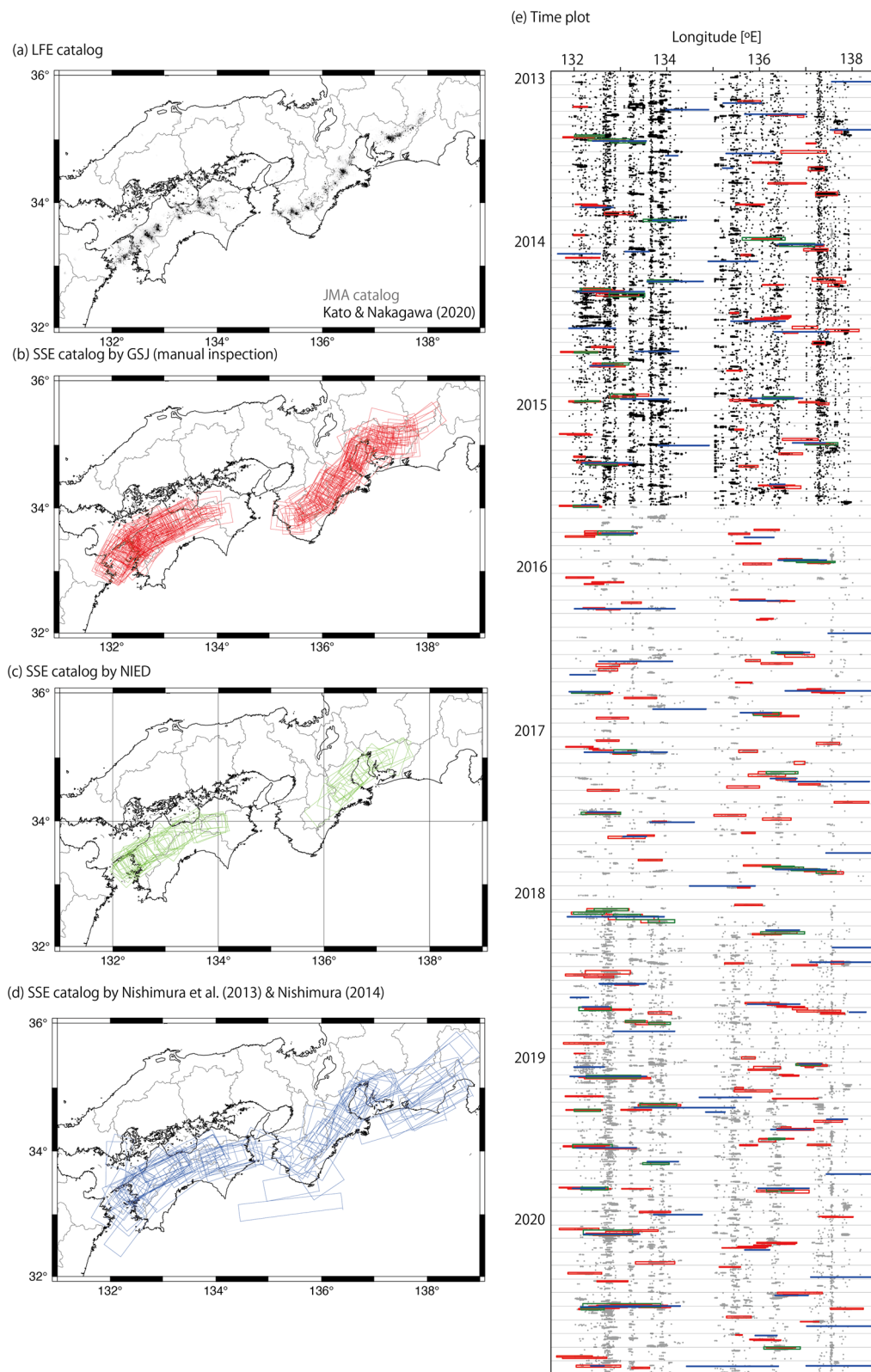
Fig. 2 LFE and SSE catalogs during 2013–2020. **a** LFE catalogs by JMA (gray) and Kato and Nakagawa ([2020]) (black). **b** SSE catalog by GSJ. **c** SSE catalog by NIED. **d** SSE catalog based on GNSS records (Nishimira et al. [2013]; Nishimura [2014]). **e** Time plots of events shown in **a**–**d**

Yabe *et al. Earth, Planets and Space* (2023) 75:13

Page 7 of 21

Method

This section presents a methodology to quantitatively detect possible short-term SSE signals from the strain and tilt data. We developed a geodetic-matched filter technique for strain and tilt data based on Nishimura et al. (2013) and Nishimura (2014). It was assumed that tectonic events occurred at some locations on the plate interface, and data fitting was conducted for the slip amount and linear trends in the data. Comparing the AIC between the models with and without the assumed tectonic deformation, possible SSEs were detected when the ΔAIC falls below a threshold value. Owing to the negative effects of temporal variations in the strain and tilt data quality, prior information on the variance in data fitting was introduced. This enabled temporal variations in data quality at individual stations to be treated.

Data selection

Additional file 2: Figure S1 shows the histograms of differential strain and tilt data after BAYTAP-G preprocessing. The strain and tilt data processed by BAYTAP-G occasionally included large steps due to local seismic events, heavy rainfall, or instrument maintenance. These steps may cause misdetection in geodetic-matched filter analysis for SSEs. Therefore, the stations in each time window were removed if they had steps $> 10^{-8}$ strain for horizontal and volumetric strain, or 10^{-8} rad for tilt.

Prior distribution for variances

It was assumed that the strain and tilt data were composed of linear trends, signals of crustal deformations, and noise. Hence, when signals of crustal deformation are absent, the data are expected to be fitted by a linear function. In a typical geodetic-matched filter analysis, the variance of this linear fitting is assumed to be constant over time. However, in strain and tilt data, this variance can temporally change, owing to time-dependent data quality. The prior distributions of variance were adopted to include these temporal variations.

Two-week time periods separated by one week in between were used, same as that used in our geodetic-matched filter analysis. For each station and component, 1,000 time periods were randomly selected. A linear function was fitted to the data at each station and component. Figure 3 shows the histograms of the variances for different stations and components. The histograms of the variances are represented by log-normal distributions. Hence, a log-normal distribution was adopted for the prior distribution of the fitting variance. The averages and variances for the prior distributions of each station
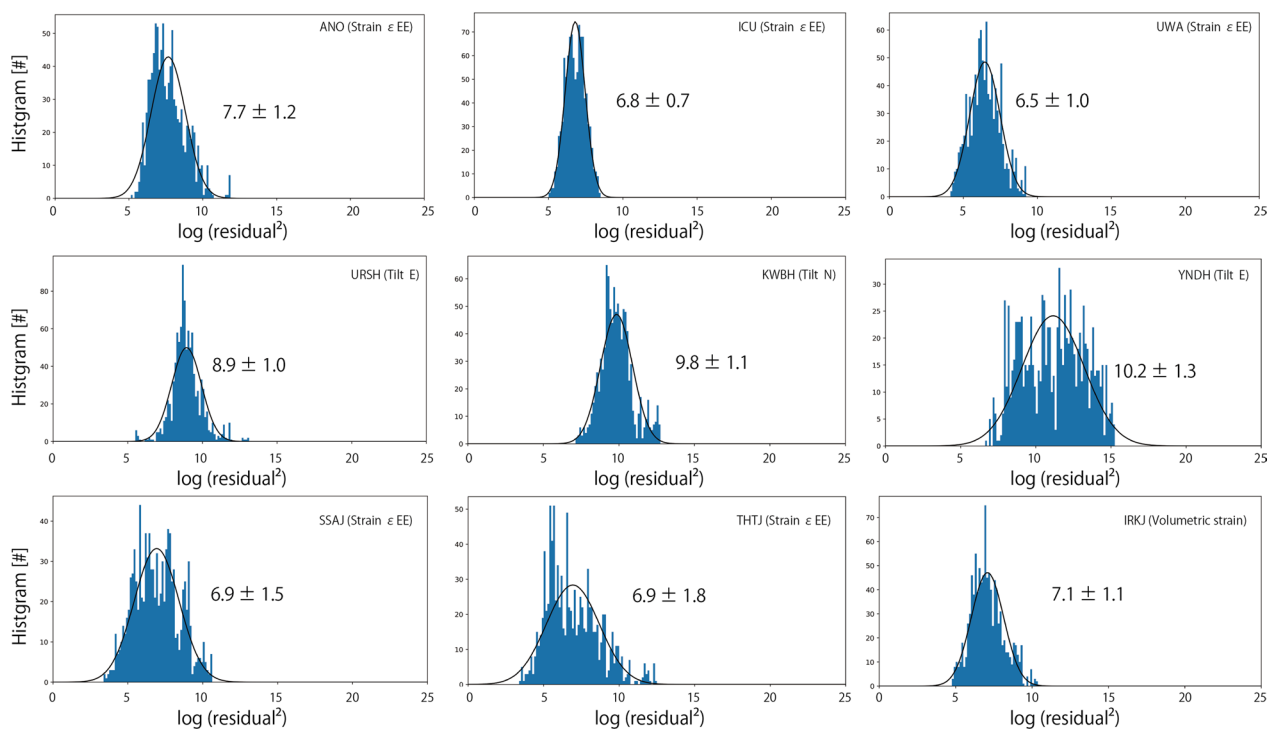

Fig. 3 Histograms of residuals for fitting a linear function to strain and tilt data. Each panel shows an example of histogram for different stations and components. Black curves represent log-normal distributions fitted for the histogram. Values in the panels are the means and standard deviations of the fitted log-normal distributions

and component were calculated based on the histogram in Fig. 3.

Geodetic-matched filter analysis for short-term SSE detection

This study developed a geodetic-matched filter analysis technique for strain and tilt data based on Nishimura et al. (2013) and Nishimura (2014). They used a step function in the middle of the time windows to represent the occurrences of SSEs. The GNSS data contained one sample per day, which did not record the detailed SSE slip evolution. However, in this study, using one sample per hour, the strain and tilt data should contain detailed SSE slip evolution. Therefore, using simple step or ramp functions is not appropriate for representing SSEs in time periods. Therefore, in this study, 2-week time periods were used, with a 1-week interval in the middle. It was assumed that SSEs occurred within one week in the middle, and data of which were not used in the fitting. One week data before and after the assumed SSEs were considered to include only common linear trends and static offsets owing to the assumed SSEs. Hence, the proposed method was formulated as follows. The observed data for the ith station and jth component of data, x_{ij} can be written as:

$$x_{ijk} = a_{ij}t_k + b_{ij} + G_{ij}H(t_k - t_{1.5N}) + e_{ijk},\qquad(1)$$

where $k = 1, \dots, N, 2N + 1, \dots, 3N$, with $N = 168$ (i.e., one week of data with one sample per hour), which represents the data point in the time domain; t_k represents the time (days); a_{ij} and b_{ij} represents coefficients for a linear trend in data; G_{ij} is the static deformation due to SSEs; $H()$ is the Heaviside step function, and $t_{1.5N}$ represents the timing of the middle of time windows; e_{ijk} represents Gaussian noise with variance σ_{ij}^2. The deformation was calculated using Okada (1992) code, assuming a rigidity of 41 GPa and a Poisson ratio of 0.25. The fault was assumed to be on the plate interface based on Baba et al. (2002), Nakajima and Hasegawa (2007), and Hirose et al. (2008). This results in detecting the crustal deformation only caused by faulting on the plate interface. The fault size was assumed to be 20 km along both the strike and dip directions. The strike and dip of the fault were calculated based on the interpolation of the plate interface model. The slip direction (i.e., rake) was assumed to be parallel to the subduction direction of the Philippine Sea Plate (Miyazaki and Heki 2001). The fault searching location grid size was 0.1° in latitude and longitude. The depth of the fault location was constrained to 15–50 km. The slip quantity was also grid-searched from 0–100 mm at 10 mm intervals.

The conditional probability $P\left(x_{ij}|\sigma_{ij}^2\right)$ can be written by the normal distribution as:

$$P\left(x_{ij}|\sigma_{ij}^2\right) = \frac{1}{\left(2\pi\sigma_{ij}^2\right)^{0.5}}exp\left[-\frac{\sum_k e_{ijk}^2}{2\sigma_{ij}^2}\right].\qquad(2)$$

Hence, the coefficients for the linear trend were estimated in the least-squares sense. The prior distribution for the variance $P\left(\sigma_{ij}^2\right)$ was assumed to be a log-normal distribution, as follows:

$$P\left(\sigma_{ij}^2\right) = \frac{1}{\sqrt{2\pi}\,\tau_{ij}\sigma_{ij}^2}exp\left[-\frac{\left(\log\sigma_{ij}^2 - \mu_{ij}\right)^2}{2\tau_{ij}^2}\right],\qquad(3)$$

where μ_{ij} and τ_{ij}^2 are the average and variance of the log-normal distribution, respectively. The log likelihood is then calculated by:

$$L_{ij} = \log\int_{-\infty}^{\infty}P\left(x_{ij}|\sigma_{ij}^2\right)P\left(\sigma_{ij}^2\right)d\left(\log\sigma_{ij}^2\right).\qquad(4)$$

For the model without crustal deformation (i.e., zero slip), the AIC was calculated by considering all stations and all components as:

$$AIC = -2\sum_{ij}\left(L_{ij} - 2\right).\qquad(5)$$

For the model with crustal deformation (i.e., positive slip), the AIC was calculated in the same manner as:

$$AIC = -2\sum_{ij}\left(L_{ij} - 2\right) + 2.\qquad(6)$$

For every time window and spatial grid for the fault location, grid searches were conducted for the slip amount. Then, the model with the minimum AIC value was selected as the best model. The time windows were shifted every 24 h during the analysis period between 2013 and 2020.

The developed method can detect crustal deformation similar to that caused by known short-term SSEs in this region. For example, we constrained source locations of possible events on the plate interface. If the crustal deformation occurs by other tectonic reasons (for example, aseismic creep on crustal faults), they are rejected as noises or projected onto the artificial sources on the plate interface. We also assumed a duration of less than one week for the possible events, based on the past short-term SSE and LFE activities in

Yabe *et al. Earth, Planets and Space*   (2023) 75:13

Page 9 of 21

this region. According to the GSJ catalog, durations of typical short-term SSEs are usually less than one week. For larger events with significant source migration, although the entire durations of such events are sometimes longer than one week, slip on the particular fault plane is usually less than one week. If there are aseismic slip on the plate interface with long duration (unknown aseismic transients or long-term SSEs), such events are difficult to be detected with this method. Therefore, to explore the possibilities of other tectonic events, it is necessary to conduct grid searches for source location and geometry and event duration.

Event selection and final fault model estimation

Using the temporal and spatial distributions of the calculated ΔAIC, possible SSEs were detected. First, the minimum ΔAICs of certain locations and times were selected; these were among those values within ± three days and ± 0.3° in latitude and longitude. Among these selected points, if less than three stations contributed to more than 90% of the likelihood differences, they were rejected, because we considered that tectonic events should be recorded at more than two stations. Finally, only the points with a ΔAIC less than − 6.0 were considered candidates of short-term SSE events.

The final fault models for the detected short-term SSE candidates were constructed. In the detection algorithm, the duration of the SSEs was fixed to one week. The appropriate duration of the event was defined by grid search around the detection time with one day interval. The fault sizes were estimated by grid searching around the detected location using the defined SSE duration. The search was within a length of 10–100 km along the strike and a width of 10–50 km along the dip, and both were at 10 km intervals. Finally, the slip amount was detected by grid search (1–100 mm, at 1 mm intervals) using the defined SSE duration and fault sizes.

Results and discussion

This study developed an objective method to detect possible short-term SSEs from tilt and strain records. This method was previously used for GNSS records to construct long-term catalogs (Nishimura et al. 2013; Nishimura 2014); however, there are no such catalogs using tilt and strain records. As subjective detection criteria can vary, according to different analysts and/or different times, it is more suitable to use objective detection methods to construct long-term event catalogs.

In this study, 130 events were detected over a period of eight years using the quantitative detection method of SSEs from tilt and strain data. Additional files 3, 4, 5, 6, and 7: Figures S2–S6 show examples of data and detected

events in different regions. Strain and tilt data showed transient deformation when LFE activities occurred in nearby regions. No heavy rainfall was observed at nearby Automated Meteorological Data Acquisition System stations (AMEDAS). The source locations of the detected SSEs coincided with the LFE hypocenters. The spatio-temporal coincidences with LFE activities suggest that the detected crustal deformations are caused by SSEs. Transient deformation signals during the middle one week fluctuated with time, suggesting that they represent spatio-temporal distribution of SSE slips. Detailed studies on such features are left for the future. Additional file 1: Movie S1 shows the spatio-temporal distributions of calculated − ΔAIC values. Figure 4 shows the calculated − ΔAIC values projected on a longitudinal axis. The detected events were usually followed by active LFEs, suggesting that a large portion of these detections are SSEs. Some large − ΔAIC values are not marked as detections, indicating that these values were caused by a residual reduction at less than three stations. The removed events may represent small SSEs which were observed only at a few stations or noise signals whose deformation patterns were similar to those due to slip on the plate interface. Figure 5 shows the spatial distributions of negative ΔAIC values stacked for spatio-temporal grids. Large stacked values were observed along the tremor zone (Fig. 2), which also suggests that a large portion of the detections are SSEs. The final fault models of 130 detected events were estimated, as summarized in Tables S1 and S2. Figure 6 shows the spatial distribution of the estimated final fault models. More than 80 events were located along the tremor zone, although some events were located up-dip or down-dip of the tremor zone. Timings of such irregular events occasionally corresponded to periods with heavy rainfall (> 50 mm/d). Figure 6 shows 23 events in gray rectangles, which represent the events in which heavy rainfall (> 50 mm/d) occurred during event periods at the AMEDAS stations close to the tilt or strain stations, with the largest log-likelihood reduction. Additional file 8: Figure S7 shows an example of the data and detected events during such heavy rainfall periods. Transient changes occurred in strain data when heavy rainfall was observed. Detection was not coincident with LFE activities. Therefore, we interpreted that such events are not tectonic signals, but artificial detection due to heavy rainfalls. Figure 7 shows the spatio-temporal distribution of detected events. Events detected during the period of heavy rainfall were removed in the following analysis.

Figure 2 presents the detection results of the other catalogs. The GSJ, NIED, and GNSS catalogs contained 265, 53, and 87 SSEs, respectively, during the study period. However, their SSEs sometimes represent
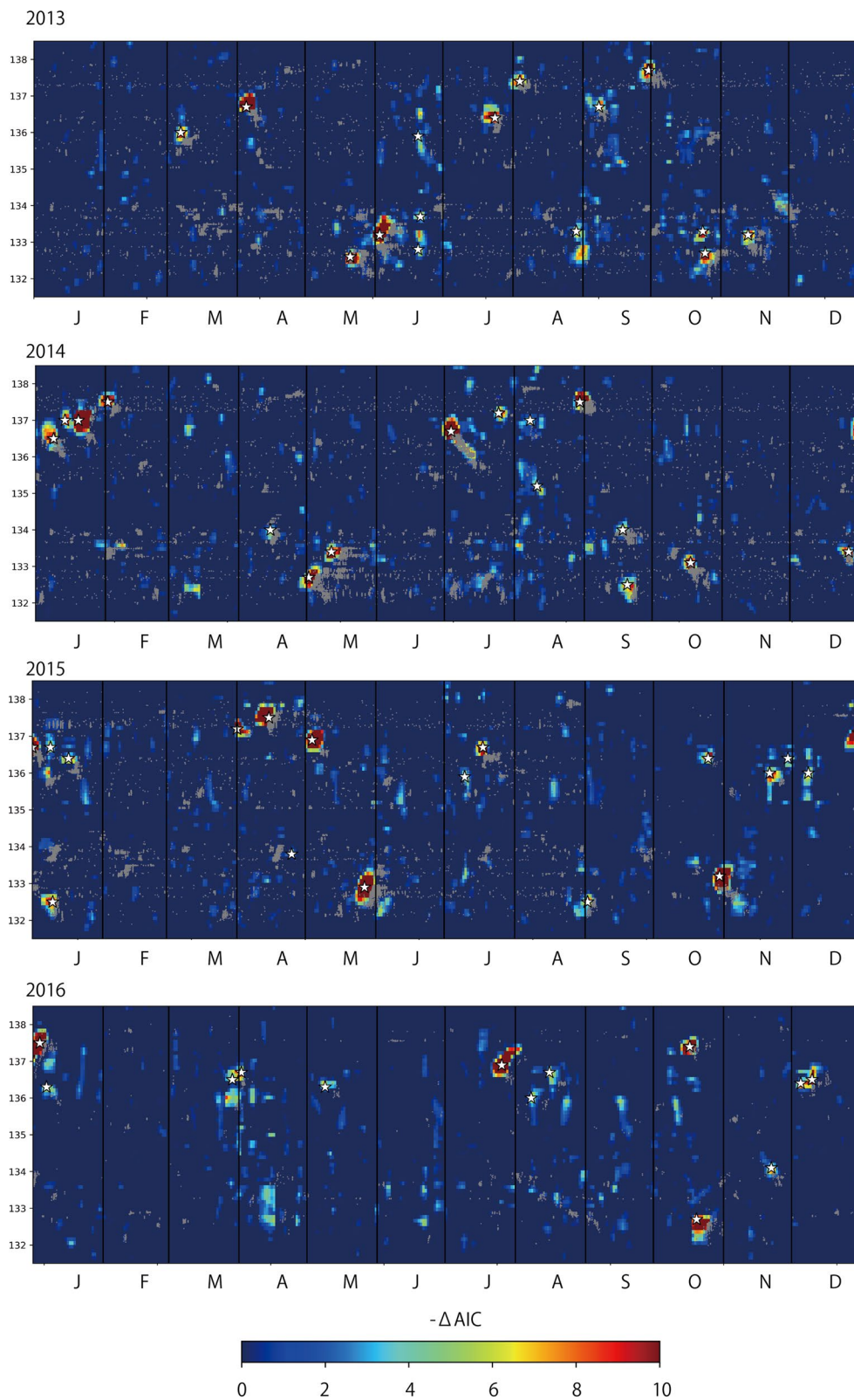
Yabe *et al. Earth, Planets and Space* (2023) 75:13

Page 10 of 21

Fig. 4 Temporal–spatial distributions of the calculated ΔAIC. Background colors represent the calculated ΔAIC. White stars represent the timings and locations of events detected in this study. Gray dots are LFEs by JMA and Kato and Nakagawa (2020)
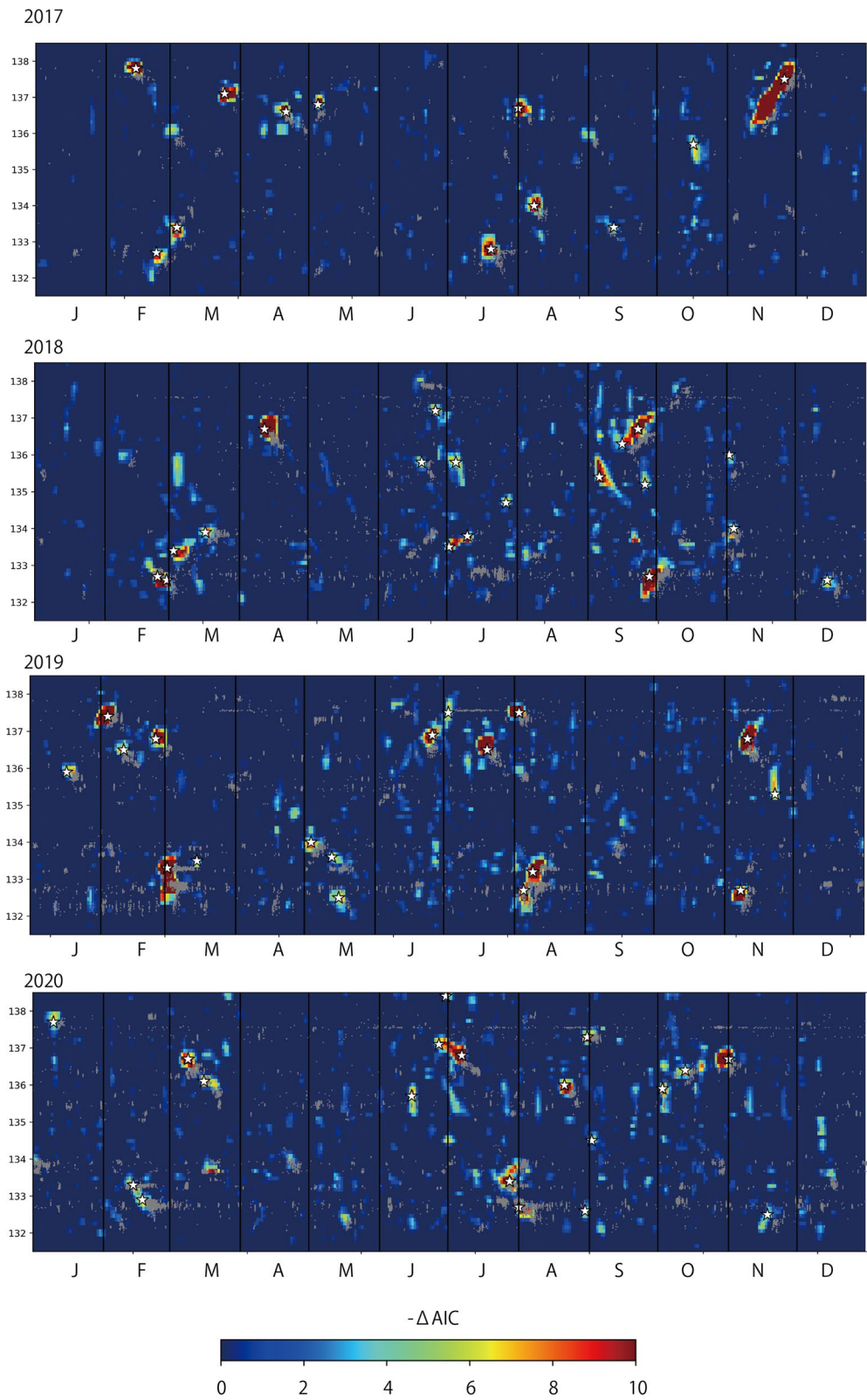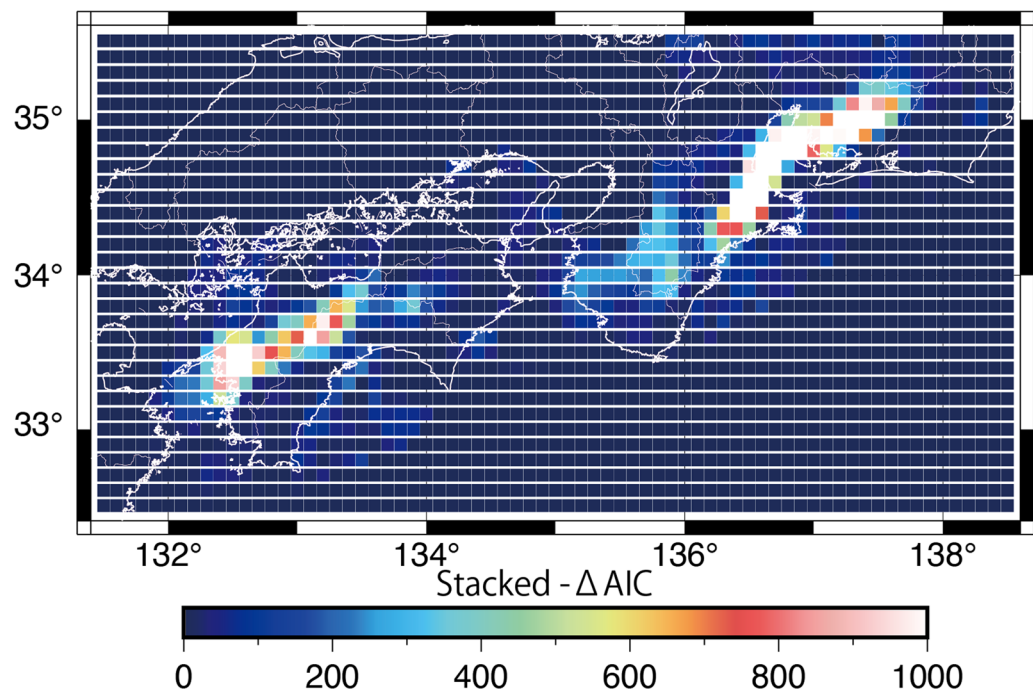
Fig. 4 continued

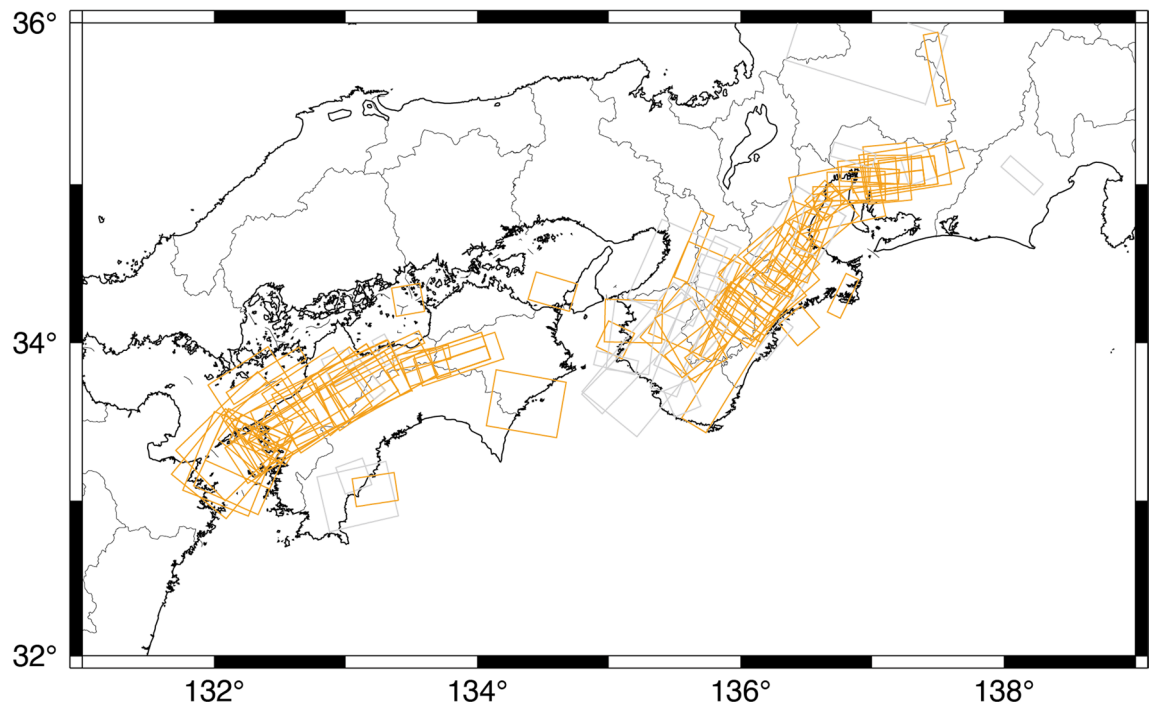**Fig. 5** Spatial distributions of stacked — ΔAIC values

Fig. 6 Spatial distributions of detected events in this study. Orange squares are detected possible SSEs. Gray squares are events detected in the period of heavy rainfalls (> 50 mm/d)
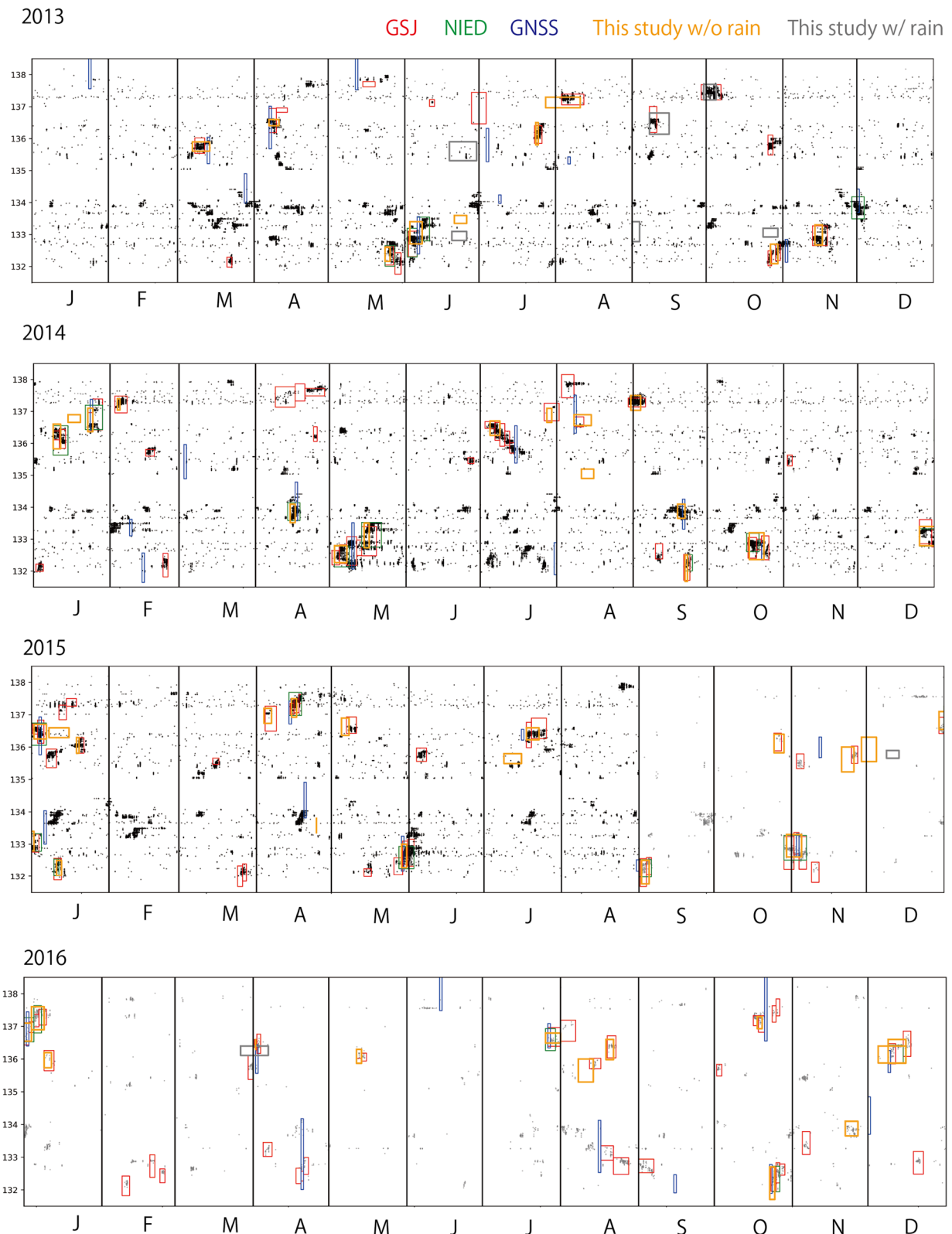
Fig. 7 Temporal distributions of detected events in four catalogs. Red, green, blue, and orange rectangles represent events in catalogs of GSJ, NIED, GNSS, and this study, respectively. Gray and black dots represent LFE catalogs of JMA and Kato and Nakagawa (2020), respectively
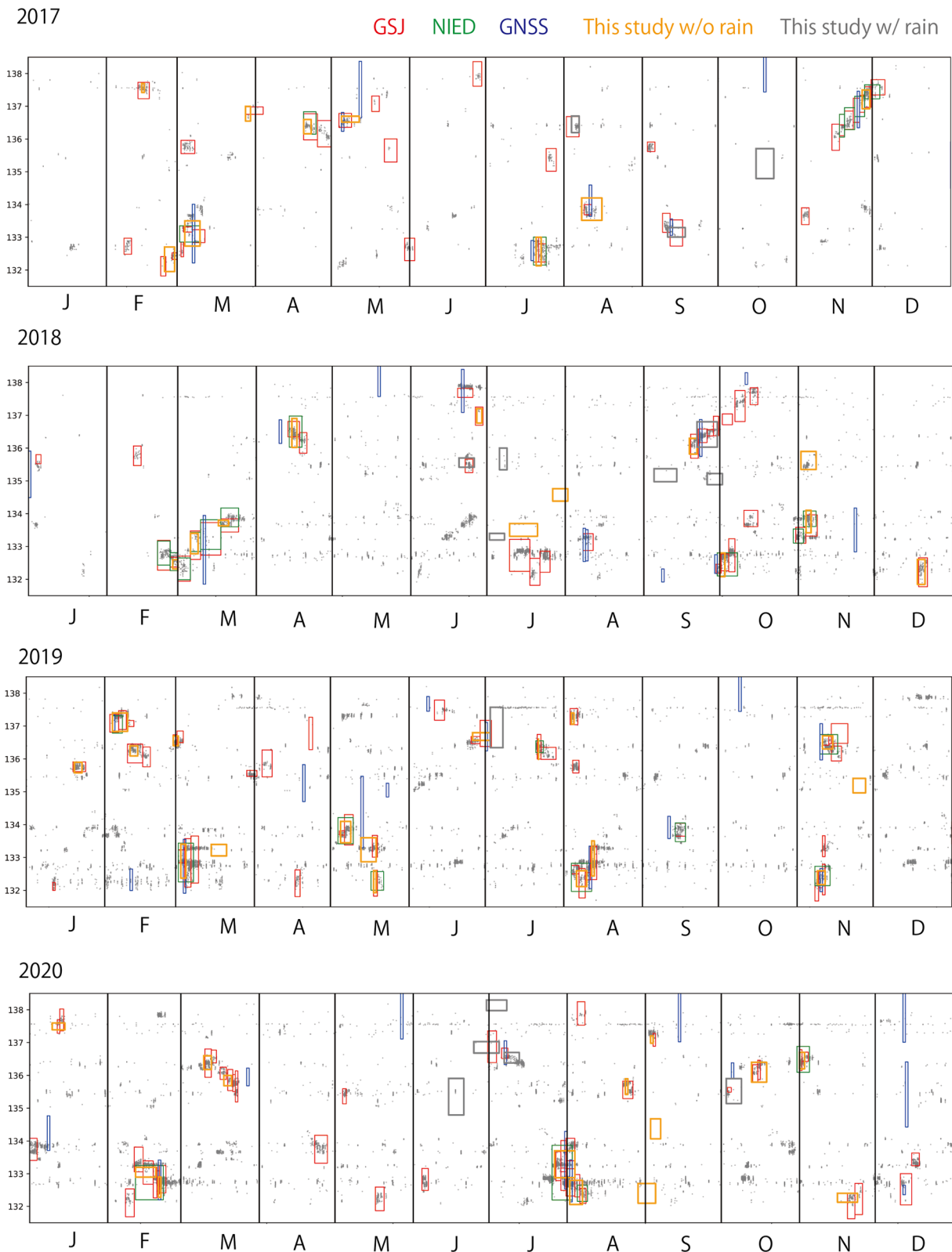
Fig. 7 continued

Yabe *et al. Earth, Planets and Space*   (2023) 75:13

Page 15 of 21

subevents of large, single SSEs. Therefore, each catalog was summarized by focusing on the main events, as shown in Additional file 10: Table S1. The GSJ, NIED, and GNSS catalogs contained 148, 39, and 85 main events, respectively. The NIED and GSJ catalogs were very similar; 37 of 39 events in the NIED catalog were also listed in the GSJ catalog. The two missing events are SSEs in the eastern Shikoku region (event numbers 26 and 38 in Additional file 10: Table S1). The NIED is based on tilt records only, while the GSJ catalog is based on strain and tilt records. Therefore, the GSJ catalog detected more events than the NIED catalog. On the other hand, the GNSS catalog overlapped with the GSJ catalog; 49 of 85 events in the GNSS catalog were also listed in the GSJ catalog. This study detected 96 events, of which 78 events are also listed in the GSJ catalog. The method introduced in this study can detect more events in the GSJ catalog than in the NIED and GNSS catalogs. The estimated moments of overlapping events among the four catalogs were compared and the results showed consistency (Fig. 8). Figure 9 summarizes the cumulative number of events in each catalog as a function of event size. This shows that the NIED and GNSS catalogs saturated at approximately Mw 5.8–6.0, whereas the catalog of this study saturated at a low magnitude of approximately Mw 5.6–5.8. The GSJ catalog saturated at an even lower magnitude of Mw 5.3–5.5. Although less than the detection threshold, our method sometimes results in a peak of $-\Delta$AIC values during periods of small events (for example, the end of October, 2013 at western part of Kii Peninsula). Crustal deformation signals of such small events are small, and only a few stations can capture their signals. Therefore, $-\Delta$AIC values tend to be smaller for such events.

However, we did not decrease the detection threshold value as it increases the number of artificial detections.

Among the events listed in this study and the GNSS catalog, 18 and 36 events were not listed in the GSJ catalog, respectively. Figure 10 shows the spatial distribution of these events. From this study's catalog, the timing of events that overlapped with the GSJ catalog did not almost correspond to heavy rainfall (Fig. 10a). However, a large portion of events which corresponded with heavy rainfall did not overlap with the GSJ catalog (Fig. 10b). Several events detected in the Eastern Shikoku regions and not listed in the GSJ catalog are synchronized with tremor activities (Figs. 10b and S3; event numbers 38, 50, and 103 in Additional file 10: Table S1) and sometimes detected by the GNSS or NIED catalogs, suggesting that these events could be genuine SSEs.

Several studies (Kano et al. 2019; Kano and Kato 2020; Kita et al. 2021) suggest the possibility of aseismic events shallower than regular SSEs. Our detection results include several such candidates at shallow depths (Figs. 6 and 10b). Although most of them corresponded to heavy rainfall, some events are not coincident with heavy rainfalls. Additional file 9: Figure S8 shows an example of such data and detected events; transient changes in data are coincident with moderate rainfall but not with LFE activities. The GNSS records were also examined for events with magnitudes > 6.0, to confirm the existence of such events. As GNSS catalog of short-term SSEs can detect mainly events with magnitude ~ 6.0 or larger as discussed earlier, we expect that such events are visible in GNSS records. However, there were not any obvious indications of these events in the GNSS records (Additional file 9: Figure S8). Therefore, many such events may not be tectonic deformations, but rather the artificial
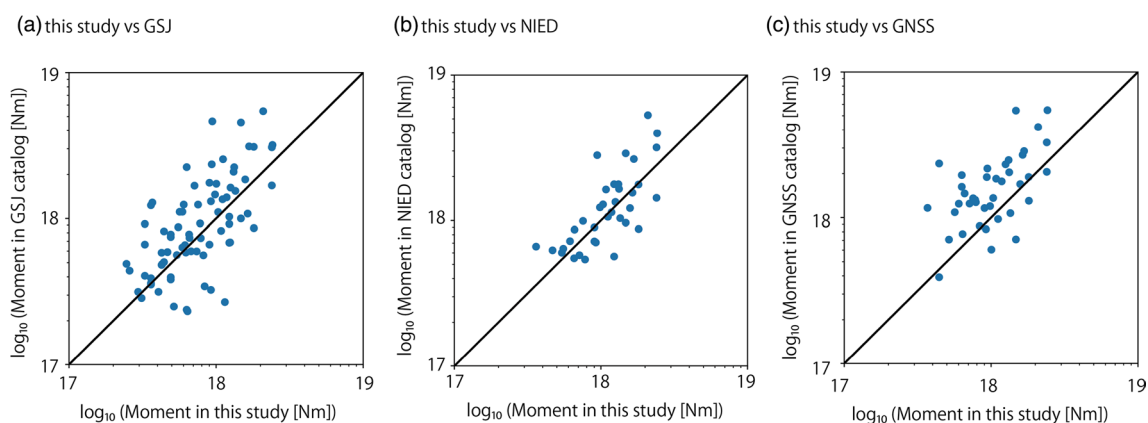

Fig. 8 Comparisons of seismic moments in different catalogs. **a** Comparisons between GSJ catalog and a catalog of this study. **b** Comparisons between NIED catalog and a catalog of this study. **c** Comparisons between GNSS catalog and this study's catalog
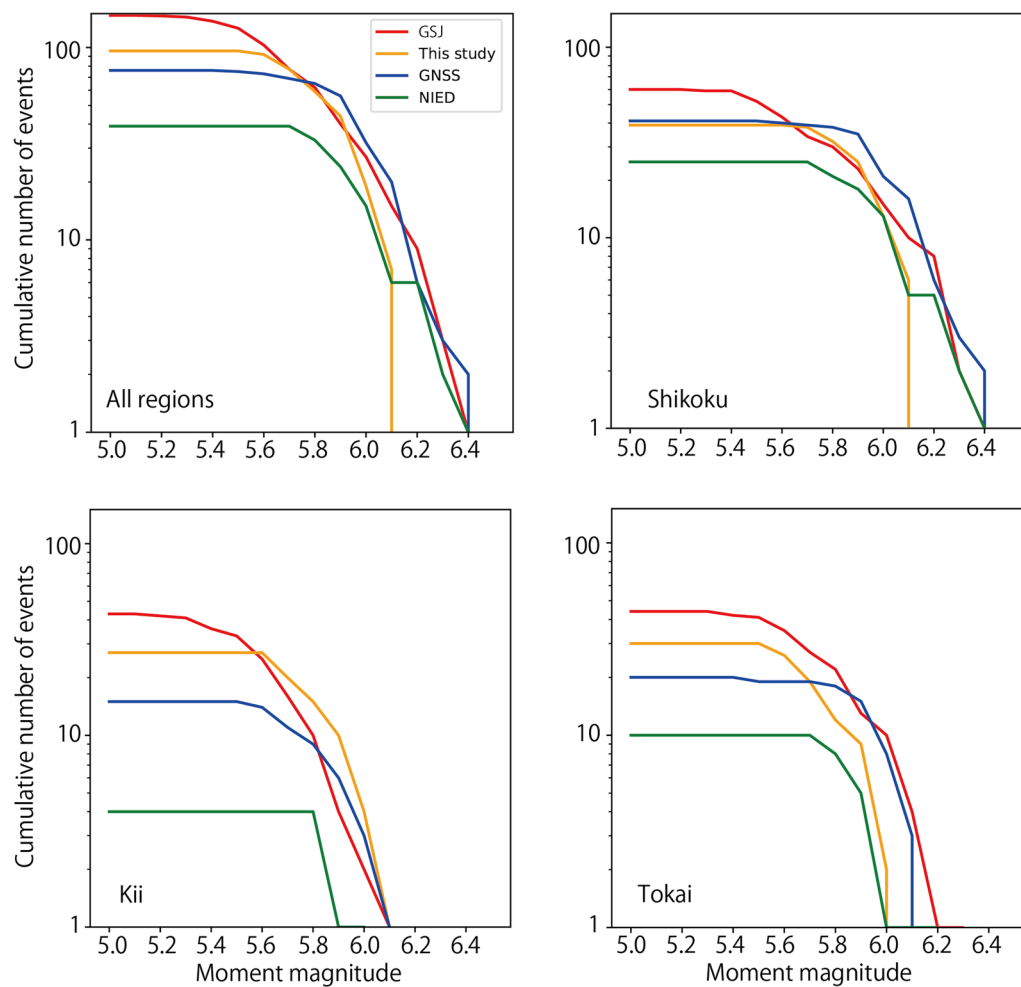
Fig. 9 Cumulative number of events against moment magnitude. Red, green, blue, and orange curves represent the catalogs of the GSJ, NIED, GNSS, and this study, respectively

detection owing to other causes, regardless of introducing log-normal fittings prior distributions in the developed method.

For the GNSS catalog, events not overlapping with the GSJ catalog were concentrated in two regions (Fig. 10d; the Eastern Shikoku region near the Kii Channel, and the Eastern Tokai region, which is shallower than the regular SSE region). Only a few events were detected in the Eastern Shikoku region in the GSJ catalog (Fig. 2b) and the catalog developed in this study (Fig. 6). In this region, the detectability of SSEs using strain and tilt records could be low because Ishii-type strainmeters were not deployed; additionally, the quality of tilt records was poor. In contrast, the detectability of SSEs in the Eastern Tokai region (shallower than regular SSE regions) should be high because there are many volumetric and horizontal

strainmeters deployed in this region. According to Okada et al. (2022), the typical duration of SSEs in this region is longer (> 15 days) than that of regular SSEs, with a low slip rate, which may make it difficult to detect such events using strain and tilt data.

Figure 11 shows the time evolution of moment release. The cumulative moment release in the 8-year study period appears different among the four catalogs referred to in this study. In the Shikoku region, the GSJ and GNSS catalogs showed large cumulative moment release, whereas the other two catalogs showed low cumulative moment release (approximately half of the GSJ and GNSS catalogs). In the Kii region, the GSJ catalog and results of this study showed a similar time evolution of moment release; however, the NIED catalog showed very low values. In the Tokai region, the GSJ catalog showed
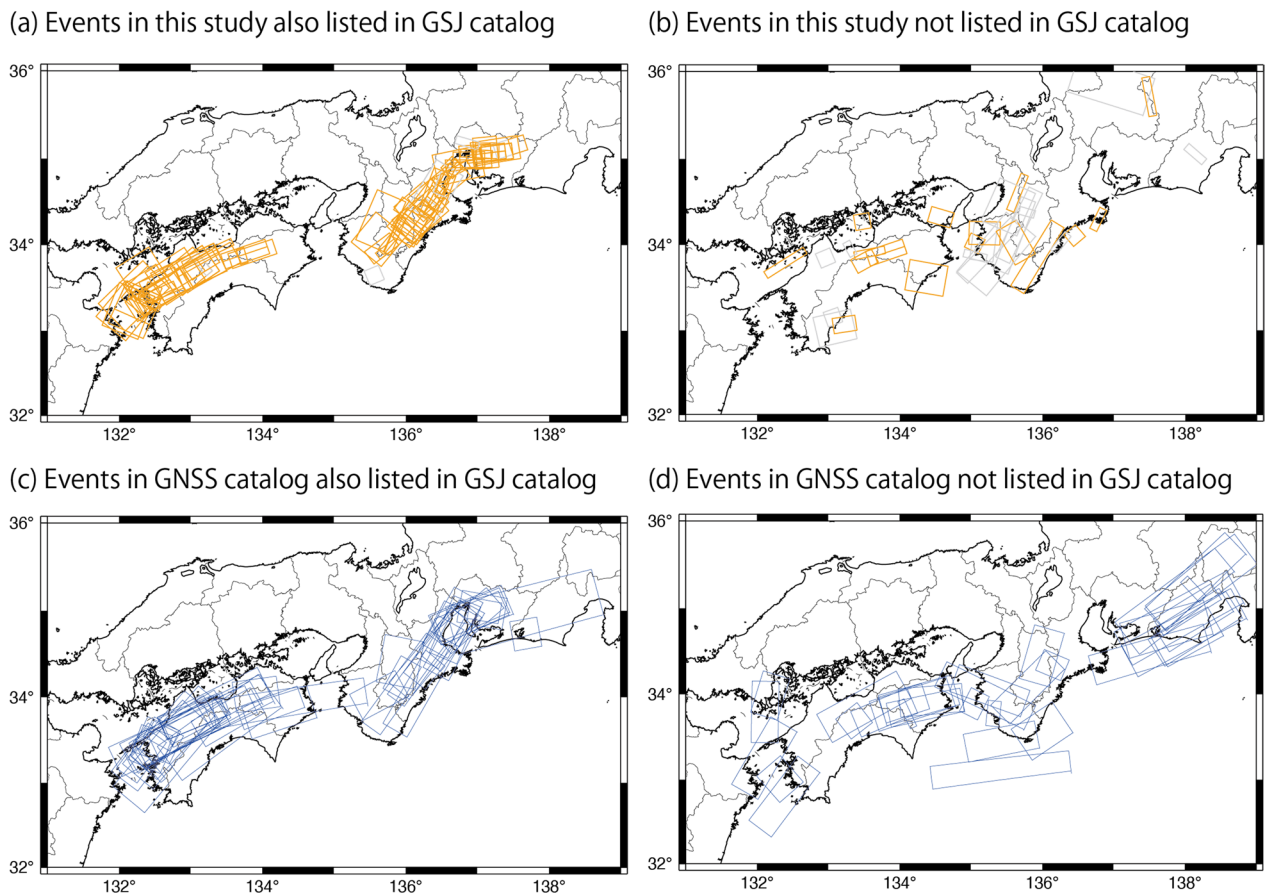
Yabe *et al. Earth, Planets and Space*   *(2023) 75:13*

Page 17 of 21

(a) Events in this study also listed in GSJ catalog

(b) Events in this study not listed in GSJ catalog

(c) Events in GNSS catalog also listed in GSJ catalog

(d) Events in GNSS catalog not listed in GSJ catalog

Fig. 10 Spatial distributions of fault models of events in the catalogs of this study and GNSS. **a** Fault models of events in the catalogs of this study and GSJ. **b** Fault models of events in this study's catalog, but not listed in the GSJ catalog. **c** Fault models of events in the GNSS and GSJ catalogs. **d** Fault models for events in the GNSS catalog, but not in the GSJ catalog
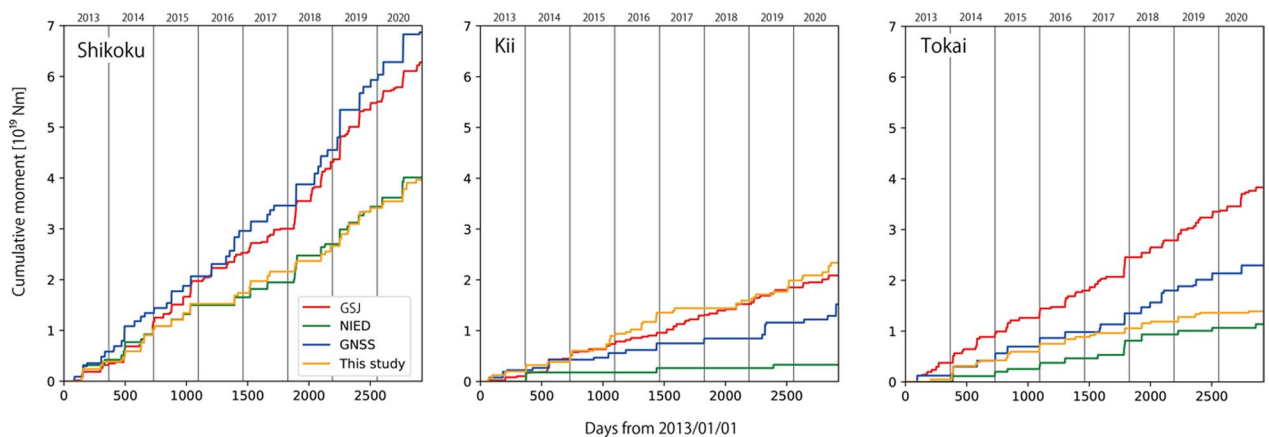

Fig. 11 Time evolution of moment release listed in catalogs. Red, green, blue, and orange lines represent catalogs of the GSJ, NIED, GNSS, and this study, respectively. Three panels show results for the Shikoku regions, Kii region, and Tokai region, respectively

the largest cumulative moment release. The GNSS catalog and results of this study showed a similar time evolution of moment release at the start of the study period. However, they deviated approximately half-way through the period (~ May 2017). The NIED catalog had the lowest value in this region. Therefore, it should be noted that short-term SSE catalogs have such uncertainties. Detailed comparisons of short-term SSE catalogs should be conducted in future studies.

Conclusions

This study monitored the short-term SSEs in southwest Japan to understand the spatial and temporal distributions of slip deficit accumulation at the plate interface. Due to the small magnitude events in southwest Japan, the detectability of SSEs with GNSS records is limited, and strain and tilt records have been used as an alternative. Although SSE catalogs have been constructed by GSJ using strain and tilt records, their detection of events is based on subjective criteria because of spatial and temporal changes in data quality, which are not suitable for constructing a unified long-term catalog. In this study, we developed a quantitative method for detecting SSEs from strain and tilt records and constructed a long-term catalog for the period 2013–2020. This catalog detected 96 candidate SSEs over 8 years. Comparing the catalogs of this study and GSJ, SSEs with a magnitude of > 5.8 in the GSJ catalog are included in our catalog. However, many small events in the GSJ catalog are not included in our catalog, suggesting that small events are difficult to distinguish from noise, which synchronize with tremor activities by chance. This study's catalog also included events deeper and shallower than those of the tremor zones, which were not included in the GSJ catalog. Although the existence of such deeper or shallower slips was also suggested by previous studies, the timing of such events mostly corresponded to heavy rainfall. This suggests that they are artificially detected, regardless of the introduction of log-normal prior distribution in the developed method. Such differences in the short-term SSE catalogs indicate that short-term SSE catalogs have such uncertainties and we should be aware of them.

Abbreviations

GSJ	Geological Survey of Japan
NIED	National Research Institute for Earth Science and Disaster Resilience
JMA	Japan Meteorological Agency
SSE	Slow slip event
GNSS	Global Navigation Satellite System
CCEP-J	Coordinating Committee for Earthquake Prediction, Japan
AIC	Akaike's information criteria
GTSM	Gladwin Tensor Strainmeter
LFE	Low-frequency earthquake
AMEDAS	Automated Meteorological Data Acquisition System

Supplementary Information

The online version contains supplementary material available at https://doi.org/10.1186/s40623-023-01769-9.

Additional file 1: Movie S1. A movie showing spatio-temporal distributions of -ΔAIC and LFEs. Background color represents -ΔAIC values in each grid. Gray dots are LFEs in catalogs of JMA and Kato and Nakagawa (2020). Red rectangles are SSE fault models of events in the GSJ catalog.

Additional file 2: Figure S1. Examples for step size distributions of strain and tilt data. Red lines show the data-selection thresholds.

Additional file 3: Figure S2. An example of strain and tilt data for the detected events in western Shikoku region. The top panel shows the spatial distribution of likelihood changes at each station. Green dots are LFEs by JMA. The purple square is the fault grid of the detected event. The above detection occurred on May 2, 2014. Four panels in the middle show strain and tilt data for stations with top 4 likelihood changes among used stations. The middle one week, marked by two black vertical lines, is the assumed period for possible SSEs, which was not used for data fitting. Colored curves are observed data, and black solid lines are data fitting by the developed method. Black dashed lines in the middle one week shows static offsets estimated by the developed method. Below the four panels, temporal evolutions of rainfall and LFE activities are shown. The location of rainfall station is represented by the orange square in the map. The bottom panel is the temporal distribution of calculated ΔAIC values at the detected grid location.

Additional file 4: Figure S3. An example of strain and tilt data for the detected event in eastern Shikoku region. Legends are same as Figure S2.

Additional file 5: Figure S4. An example of strain and tilt data for the detected event in western Kii Peninsula. Legends are same as Figure S2.

Additional file 6: Figure S5. An example of strain and tilt data for the detected event in eastern Kii Peninsula. Legends are same as Figure S2.

Additional file 7: Figure S6. An example of strain and tilt data for the detected event in Tokai region. Legends are same as Figure S2.

Additional file 8: Figure S7. An example of strain and tilt data for the detected event during the period with heavy rainfalls. Legends are same as Figure S2.

Additional file 9: Figure S8. An example of strain and tilt data for the detected event and comparisons with GNSS data. Legends are same as Figure S2. Additional panels for GNSS data (baseline length of the GNSS stations between Maizuru and Naruto) are shown at the bottom.

Additional file 10: Table S1. A list of SSEs in four catalogs (GSJ, NIED, GNSS, and this study).

Additional file 11: Table S2. Source parameters of SSEs detected in this study.

Author contributions
YK, SI, NM, and TM contributed to data acquisition and preprocessing. SY conducted analysis and drafted manuscript. TO contributed to interpretations. All authors read and approved to the final manuscript.

Yabe *et al. Earth, Planets and Space*   (2023) 75:13

Page 19 of 21

Availability of data and materials
The tiltmeter data of the NIED can be obtained from the Hi-net webpage (https://www.hinet.bosai.go.jp) via a data inquiry form. Strain data from AIST are available from the corresponding author upon request. The SSE catalog of this study is provided in (Additional file 11: Table S2).

Declarations

Ethics approval and consent to participate
Not applicable.

Consent for publication
Not applicable.

Competing interests
The authors declare that they have no competing interests.

Author details
[1]Geological Survey of Japan, National Institute of Advanced Industrial Science and Technology, Tsukuba Central 7, 1-1-1 Higashi, Tsukuba, Ibaraki 305-8567, Japan. [2]National Research Institute for Earth Science and Disaster Resilience, 3-1 Tenoudai, Tsukuba, Ibaraki 305-0006, Japan.

References
Ammon CJ, Ji C, Thio HK, Robinson D, Ni S, Hjorleifsdottir V, Kanamori H, Laym T, Das S, Helmberger D, Ichinose G, Polet J, Wald D (2005) Rupture process of the 2004 Sumatra-Andaman earthquake. Science 308(5725):1133–1139. https://doi.org/10.1126/science.1112260

Ando M (1975) Source mechanism and tectonic significance of historical earthquakes along the Nankai trough. Japan Tectonophysics 27(2):119–140. https://doi.org/10.1016/0040-1951(75)90102-X

Ando R, Imanishi K (2011) Possibility of Mw 9.0 mainshock triggered by diffusional propagation of after-slip from Mw 7.3 foreshock. Earth Planets Space 63(7):767–771. https://doi.org/10.5047/eps.2011.05.016

Asai Y, Ishii H, Aoki H (2009) Comparison of tidal strain changes observed at the borehole array observation system with in situ rock properties in the Tono region, central Japan. J Geodyn 48(3–5):292–298. https://doi.org/10.1016/j.jog.2009.09.024

Baba T, Tanioka Y, Cummins PR, Uhira K (2002) The slip distribution of the 1946 Nankai earthquake estimated from tsunami inversion using a new plate model. Phys Earth Planet Inter 132:59–73. https://doi.org/10.1016/S0031-9201(02)00044-4

Behr WM, Burgmann R (2021) What's down there? The structures, materials and environment of deep-seated slow slip and tremor. Phil Trans R Soc. https://doi.org/10.1098/rsta.2020.0218

Canitano A, Mouyen M, Hsu YJ, Linde A, Sacks S, Lee HM (2021) Fifteen years of continuous high-resolution borehole strainmeter measurements in eastern Taiwan: an overview and perspectives. GeoHazards 2:172–195. https://doi.org/10.3390/geohazards2030010

Chao K, Obara K (2016) Triggered tectonic tremor in various types of fault systems of Japan following the 2012 Mw 8.6 Sumatra earthquake. J Geophys Res Solid Earth 121:170–187. https://doi.org/10.1002/2015JB012566

Dragert H, Wang K, James TS (2001) A silent slip event on the deeper Cascadia subduction interface. Science 292(5521):1525–1528. https://doi.org/10.1126/science.1060152

Frank WB, Rousset B, Lasserre C, Campillo M (2018) Revealing the cluster of slow transients behind a large slop slip event. Sci Adv 4:eaat066. https://doi.org/10.1126/sciadv.aat0661

Furuya I, Fukudome I (1986) Characteristics of borehole volume strainmeter and its application to seismology. J Phys Earth 134:257–296

Gladwin MT (1984) High precision multi component borehole deformation monitoring. Rev Sci Instrumentation 55:2011–2016

Hart RHG, Gladwin MT, Gwyther RL, Agnew DC, Wyatt FK (1996) Tidal calibration of borehole strain meters: removing the effects of small-scale inhomogeneity. J Geophys Res 101:25553–25571. https://doi.org/10.1029/96JB02273

Hirose H, Kimura T (2020) Slip distributions of short-term slow slip events in Shikoku, southwest Japan, from 2001 to 2019 based on tilt change measurements. J Geophys Res Solid Earth 125:e2020JB019601. https://doi.org/10.1029/2020JB019601

Hirose H, Obara K (2006) Short-term slow slip and correlated tremor episodes in the Tokai region, central Japan. Geophys Res Lett 33:L17311. https://doi.org/10.1029/2006GL026579

Hirose H, Hirahara K, Kimata F, Fujii N, Miyazaki S (1999) A slow thrust slip event following the two 1996 Hyuganada earthquakes beneath the Bungo channel, southwest Japan. Geophys Res Lett 26(21):3237–3240. https://doi.org/10.1029/1999GL010999

Hirose F, Nakajima J, Hasegawa A (2008) Three-dimensional seismic velocity structure and configuration of the Philippine sea slab in southwestern Japan estimated by double-difference tomography. J Geophys Res 113:B09315. https://doi.org/10.1029/2007JB005274

Ide S, Yabe S (2014) Universality of slow earthquakes in the very low frequency band. Geophys Res Lett 41:2786–3279. https://doi.org/10.1002/2014GL059712

Ide S, Yabe S (2019) Two-dimensional probabilistic cell automaton model for broadband slow earthquakes. Pure Appl Geophys 176:1021–1036. https://doi.org/10.1007/s00024-018-1976-9

Ide S, Shelly DR, Beroza GC (2007a) Mechanism of deep low frequency earthquakes: Further evidence that deep non-volcanic tremor is generated by shear slip on the plate interface. Geophys Res Lett 34:L03308. https://doi.org/10.1029/2006GL028890

Ide S, Beroza G, Shelly D, Uchide T (2007b) A scaling law for slow earthquakes. Nature 447:76–79. https://doi.org/10.1038/nature05780

Ide S, Baltay A, Beroza GC (2011) Shallow dynamic overshoot and energetic deep rupture in the 2011 Mw 9.0 Tohoku-Oki earthquake. Science 332(6036):1426–1429. https://doi.org/10.1126/science.1207020

Ishii H, Yamauchi T, Matsumoto S, Hirata Y, Nakao S (2002) Development Of Multi-Component Borehole Instrument for Earthquake Prediction Study: Some Observed Examples of Precursory and Co-Seismic Phenomena Relating To Earthquake Swarms And Application Of The Instrument For Rock Mechanics. In Seismogenic process monitoring (pp. 365–377). Routledge.

Itaba S, Koizumi N, Matsumoto N, Ohtani R (2010) Continuous observation of groundwater and crustal deformation for forecasting Tonankai and Nankai earthquakes in Japan. Pure Appl Geophys 167:1105–1114. https://doi.org/10.1007/s00024-010-0095-z

Itaba S, Kitagawa Y, Koizumi N, Takahashi M, Matsumoto N, Takeda N, Kimura H, Kimura T, Matsuzawa T, Shiomi K (2013) Short-term slow slip events in the Tokai area, the Kii Peninsula and the Shikoku district, Japan (from november 2012 to april 2013). Rep Coord Comm Earthq Predict 90:254–269

Itaba S, Koizumi N, Takahashi M, Matsumoto N, Kitagawa Y, Ochi T, Takeda N, Kimura H, Kimura T, Matsuzawa T, Shiomi K (2014a) Short-term slow slip events in the Tokai area, the Kii peninsula and the Shikoku district, Japan (from may to october 2013). Rep Coord Comm Earthq Predict 91:230–242

Itaba S, Koizumi N, Takahashi M, Matsumoto N, Kitagawa Y, Ochi T, Takeda N, Kimura H, Kimura T, Matsuzawa T, Shiomi K (2014b) Short-term slow slip events in the Tokai area, the Kii Peninsula and the Shikoku district, Japan (from november 2013 to april 2014). Rep Coord Comm Earthq Predict 92:238–249

Itaba S, Koizumi N, Takahashi M, Matsumoto N, Kitagawa Y, Ochi T, Takeda N, Kimura H, Kimura T, Matsuzawa T, Shiomi K (2015) Short-term slow slip events in the Tokai area, the Kii peninsula and the Shikoku district, Japan (from may to october 2014). Rep Coord Comm Earthq Predict 93:330–335

Ito Y, Obara K, Shiomi K, Sekine S, Hirose H (2007) Slow earthquakes coincident with episodic tremors and slow slip events. Science 315(5811):503–506. https://doi.org/10.1126/science.1134454

Jahr TH (2018) Non-tidal tilt and strain signals recorded at the geodynamic observatory moxa. Thuringia Ger Geod Geodyn 9(3):229–236. https://doi.org/10.1016/j.geog.2017.03.015

Japan Meteorological Agency (2022a) 2. Crustal Strain, The Seismological Bulletin of Japan, Accessed Jan 07 2021.

Japan Meteorological Agency (2022b) 2. Crustal Strain, User's guide, The Seismological Bulletin of Japan, Accessed Jan 07 2021

Kamigaichi O, Matsumoto N, Hirose F (2021) Green's function at depth of borehole observation required for precise estimation of the effect of ocean tidal loading near coasts. Geophys J Int 227:275–286. https://doi.org/10.1093/gji/ggab216

Kaneko L, Ide S, Nakano M (2018) Slow earthquakes in the microseism frequency band (0.1–1.0 Hz) off Kii Peninsula. Jpn Geophys Res Lett 45:2618–2624. https://doi.org/10.1002/2017GL076773

Kano M, Kato A (2020) Detailed spatial slip distribution for short-term slow slip events along the Nankai subduction zone, southwest Japan. J Geophys Res Solid Earth 125:e2020JB019613. https://doi.org/10.1029/2020JB019613

Kano M, Kato A, Obara K (2019) Episodic tremor and slip silently invades strongly locked megathrust in the Nankai trough. Sci Rep 9:9270. https://doi.org/10.1038/s41598-019-45781-0

Kato A, Nakagawa S (2020) Detection of deep low-frequency earthquakes in the Nankai subduction zone over 11 years using a matched filter technique. Earth Planets Space 72:128. https://doi.org/10.1186/s40623-020-01257-4

Kato A, Obara K, Igarashi T, Tsuruoka H, Nakagawa S, Hirata N (2012) Propagation of slow slip leading up to the 2011 Mw 9.0 Tohoku-Oki earthquake. Science 335(6069):705–708. https://doi.org/10.1126/science.1215141

Katsumata A, Kamaya N (2003) Low-frequency continuous tremor around the Moho discontinuity away from volcanoes in the southwest Japan. Geophys Res Lett 30:1020. https://doi.org/10.1029/2002GL0159812

Kimura T (2013) Short-term slow slip events with non-volcanic tremor in southwest Japan (november, 2012-april, 2013). Rep Coord Comm Earthq Predict 90:412–415

Kimura T (2014) Short-term slow slip events with non-volcanic tremor in southwest Japan (november, 201-april, 2014). Rep Coord Comm Earthq Predict 92:331–337

Kimura T (2015a) Short-term slow slip events with non-volcanic tremor in southwest Japan (may, 2014-october, 2014). Rep Coord Comm Earthq Predict 93:330–335

Kimura T (2015b) Short-term slow slip events with non-volcanic tremor in southwest Japan (november, 2014-april, 2015). Rep Coord Comm Earthq Predict 94:337–343

Kimura T (2016a) Short-term slow slip events with non-volcanic tremor in southwest Japan (may, 2015-october, 2015). Rep Coord Comm Earthq Predict 95:338–343

Kimura T (2016b) Short-term slow slip events with non-volcanic tremor in southwest Japan (november, 2015-april, 2016). Rep Coord Comm Earthq Predict 96:379–382

Kimura T (2017a) Short-term slow slip events with non-volcanic tremor in southwest Japan (may, 2016-october, 2016). Rep Coord Comm Earthq Predict 97:404–408

Kimura T (2017b) Short-term slow slip events with non-volcanic tremor in southwest Japan (november, 2016-april, 2017). Rep Coord Comm Earthq Predict 98:354–359

Kimura T (2018a) Short-term slow slip events with non-volcanic tremor in southwest Japan (May, 2017-October, 2017). Rep Coord Comm Earthq Predict 99:340–342

Kimura T (2018b) Short-term slow slip events with non-volcanic tremor in southwest Japan (november, 2017-april, 2018). Rep Coord Comm Earthq Predict 100:301–306

Kimura T (2019a) Short-term slow slip events with non-volcanic tremor in southwest Japan (may, 2018-october, 2018). Rep Coord Comm Earthq Predict 101:425–429

Kimura T (2019b) Short-term slow slip events with non-volcanic tremor in southwest Japan (november, 2018-april, 2019). Rep Coord Comm Earthq Predict 102:312–316

Kimura T (2020a) Short-term slow slip events with non-volcanic tremor in southwest Japan (may, 2019-october, 2019). Rep Coord Comm Earthq Predict 103:281–288

Kimura T (2020b) Short-term slow slip events with non-volcanic tremor in southwest Japan (november, 2019-april, 2020). Rep Coord Comm Earthq Predict 104:415–420

Kimura T (2021) Short-term slow slip events with non-volcanic tremor in southwest Japan (may, 2020 - october, 2020). Rep Coord Comm Earthq Predict 105:414–419

Kimura T, Kimura H (2014) Short-term slow slip events with non-volcanic tremor in southwest Japan (may-october, 2013. Rep Coord Comm Earthq Predict 91:317–321

Kimura T, Obara K, Kimura H, Hirose H (2011) Automated detection of slow slip events within the Nankai subduction zone. Geophys Res Lett 38:L01311. https://doi.org/10.1029/2010GL045899

Kita S, Houston H, Yabe S, Tanaka S, Asano Y, Shibutani T, Suda N (2021) Effects of episodic slow slip on seismicity and stress near a subduction-zone megathrust. Nat Commun 12:7253. https://doi.org/10.1038/s41467-021-27453-8

Liu C, Linde A, Sacks I (2009) Slow earthquakes triggered by typhoons. Nature 459:833–836. https://doi.org/10.1038/nature08042

Loveless JP, Meade BJ (2016) Two decades of spatiotemporal variations in subduction zone coupling offshore Japan. Earth Planet Sci Lett 436:19–30. https://doi.org/10.1016/j.epsl.2015.12.033

Maeda T, Obara K (2009) Spatiotemporal distribution of seismic energy radiation from low-frequency tremor in western Shikoku, Japan. J Geophys Res 114:09. https://doi.org/10.1029/2008JB006043

Masuda K, Ide S, Ohta K, Matsuzawa T (2020) Bridging the gap between low-frequency and very-low-frequency earthquakes. Earth Planets Space 72:47. https://doi.org/10.1186/s40623-020-01172-8

Matsumoto N, Kamigaichi O, Kitagawa Y, Itaba S, Koizumi N (2010) In-situ Calibration of Borehole Strainmeter Using Green's Functions for Surface Point Load at a Depth of Deployment. Paper presented at AGU Fall meeting 2010, San Francisco, 13–17 December 2010

Matsumoto N, Kamigaichi O (2021) Tidal calibration of multicomponent borehole strainmeters and validation of the method using surface waves. Research Square. https://doi.org/10.21203/rs.3.rs-602970/v1

Miyaoka K, Yokota T (2012) Development of stacking method for the detection of crustal deformation —application to the early detection of slow slip phenomena on the plate boundary in the Tokai region using strain data—. Zisin 65:205–218 (**in Japanese**)

Miyazaki S, Heki K (2001) Crustal velocity field of southwest Japan: subduction and arc–arc collision. J Geophys Res 106:4305–4326. https://doi.org/10.1029/2000JB900312

Nadeau RM, Dolenc D (2005) Nonvolcanic tremors deep beneath the San Andreas Fault. Science 307(5708):389–389. https://doi.org/10.1126/science.1107142

Nakajima J, Hasegawa A (2007) Subduction of the Philippine sea plate beneath southwestern Japan: slab geometry and its relationship to arc magmatism. J Geophys Res 112:B08306. https://doi.org/10.1029/2006JB004770

Nakamura K (2006) Low-frequency earthquakes in JMA's integrated hypocenters before august, 1999. Quart J Seism 69:177–191 (**in Japanese**)

Nishide N, Hashimoto T, Funasaki J, Nakazawa H, Oka M, Ueno H, Yamada N, Sasakawa I, Maeda K, Sugimoto K, Takashima T (2000) Nationwide activity of low-frequency earthquakes in the lower crust in Japan. Paper presented at Japan Earth and Planetary Science Joint Meeting, Tokyo, 25–28 June 2000

Nishimura T (2014) Short-term slow slip events along the Ryukyu trench, southwestern Japan, observed by continuous GNSS. Prog in Earth and Planet Sci 1:22. https://doi.org/10.1186/s40645-014-0022-5

Nishimura T, Matsuzawa T, Obara K (2013) Detection of short-term slow slip events along the Nankai trough, southwest Japan, using GNSS data. J Geophys Res Solid Earth 118:3112–3125. https://doi.org/10.1002/jgrb.50222

Noda A, Saito T, Fukuyama E (2018) Slip-deficit rate distribution along the Nankai trough, Southwest Japan, with elastic lithosphere and viscoelastic asthenosphere. J Geophys Res Solid Earth 123:8125–8142. https://doi.org/10.1029/2018JB015515

Obara K (2002) Nonvolcanic deep tremor associated with subduction in southwest Japan. Science 296(5573):1679–1681. https://doi.org/10.1126/science.1070378

Obara K, Kato A (2016) Connecting slow earthquakes to large earthquakes. Science 353(6296):253–257. https://doi.org/10.1126/science.aaf1512

Yabe *et al. Earth, Planets and Space*   (2023) 75:13

Page 21 of 21

Obara K, Sekine S (2009) Characteristic activity and migration of episodic tremor and slow-slip events in central Japan. Earth Planet Space 61:853–862. https://doi.org/10.1186/BF03353196

Obara K, Hirose H, Yamamizu F, Kasahara K (2004) Episodic slow slip events accompanied by non-volcanic tremors in southwest Japan subduction zone. Geophys Res Lett 31:L23602. https://doi.org/10.1029/2004GL020848

Ochi T, Itaba S, Koizumi N, Takahashi M, Matsumoto N, Kitagawa Y, Takeda N, Kimura H, Kimura T, Matsuzawa T, Shiomi K (2015) Short-term slow slip events in the Tokai area, the Kii peninsula and the Shikoku district, Japan (from november 2014 to april 2015). Rep Coord Comm Earthq Predict 94:250–261

Ochi T, Itaba S, Koizumi N, Takahashi M, Matsumoto N, Kitagawa Y, Takeda N, Kimura H, Kimura T, Matsuzawa T, Shiomi K (2016a) Short-term slow slip events in the Tokai area, the Kii peninsula and the Shikoku district, Japan (from may 2015 to october 2015). Rep Coord Comm Earthq Predict 95:255–264

Ochi T, Itaba S, Matsumoto N, Kitagawa Y, Takeda N, Kiguchi T, Kimura H, Kimura T, Matsuzawa T, Shiomi K (2016b) Short-term slow slip events in the Tokai area, the Kii peninsula and the Shikoku district, Japan (from november 2015 to april 2016). Rep Coord Comm Earthq Predict 96:255–270

Ochi T, Itaba S, Matsumoto N, Kitagawa Y, Takeda N, Kiguchi T, Kimura H, Kimura T, Matsuzawa T, Shiomi K (2017a) Short-term slow slip events in the Tokai area, the Kii peninsula and the Shikoku district, Japan (from may 2016 to october 2016). Rep Coord Comm Earthq Predict 97:242–253

Ochi T, Itaba S, Matsumoto N, Kitagawa Y, Takeda N, Kiguchi T, Kimura H, Kimura T, Matsuzawa T, Shiomi K (2017b) Short-term slow slip events in the Tokai area, the Kii peninsula and the Shikoku District, japan (from November 2016 to April 2017). Rep Coord Comm Earthq Predict 98:263–274

Ochi T, Itaba S, Matsumoto N, Kitagawa Y, Takeda N, Kiguchi T, Kimura H, Kimura T, Matsuzawa T, Shiomi K (2018a) Short-term slow slip events in the Tokai area, the Kii peninsula and the Shikoku district, Japan (from may 2017 to october 2017). Rep Coord Comm Earthq Predict 99:243–257

Ochi T, Itaba S, Matsumoto N, Kitagawa Y, Takeda N, Kiguchi T, Kimura H, Kimura T, Matsuzawa T, Shiomi K (2018b) Short-term slow slip events in the Tokai area, the Kii peninsula and the Shikoku district, Japan (from november 2017 to april 2018). Rep Coord Comm Earthq Predict 100:165–182

Ochi T, Itaba S, Matsumoto N, Kitagawa Y, Kiguchi T, Kimura H, Kimura T, Matsuzawa T, Shiomi K (2019a) Short-term slow slip events in the Tokai area, the Kii peninsula and the Shikoku district, Japan (from may 2018 to october 2018). Rep Coord Comm Earthq Predict 101:245–257

Ochi T, Itaba S, Matsumoto N, Kitagawa Y, Kiguchi T, Kimura H, Kimura T, Matsuzawa T, Shiomi K (2019b) Short-term slow slip events in the Tokai area, the Kii peninsula and the Shikoku district, Japan (from november 2018 to april 2019). Rep Coord Comm Earthq Predict 102:184–200

Okada Y (1992) Internal deformation due to shear and tensile faults in a half-space. Bull Seismol Soc Am 82:1018–1040. https://doi.org/10.1785/BSSA0820021018

Okada Y, Nishimura T, Tabei T, Matsushima T, Horise H (2022) Development of a detection method for short-term slow slip events using GNSS data and its application to the Nankai subduction zone. Earth Planets Space 74:18. https://doi.org/10.1186/s40623-022-01576-8

Ozawa S, Murakami M, Tada T (2001) Time-dependent inversion study of the slow thrust event in the Nankai trough subduction zone, southwestern Japan. J Geophys Res 106(B1):787–802. https://doi.org/10.1029/2000JB900317

Radiguet M, Cotton F, Vergnolle M, Campillo M, Walpersdorf A, Cotte N, Kostoglodov V (2012) Slow slip events and strain accumulation in the Guerrero gap. Mexico J Geophys Res 117:B04305. https://doi.org/10.1029/2011JB008801

Roeloffs E (2010) Tidal calibration of plate boundary observatory borehole strainmeters: roles of vertical and shear coupling. J Geophys Res 115:B06405. https://doi.org/10.1029/2009JB006407

Rogers G, Dragert H (2003) Episodic tremor and slip on the Cascadia subduction zone: the chatter of silent slip. Science 300(5627):1942–1943. https://doi.org/10.1126/science.1084783

Ruiz S, Metois M, Fuenzalida A, Ruiz J, Leyton F, Grandin R, Vigny C, Madariaga R, Campos J (2014) Intense foreshocks and a slow slip event preceded the 2014 Iquique Mw 8.1 earthquake. Science 345(6201):1165–1169. https://doi.org/10.1126/science.1256074

Sekine S, Hirose H, Obara K (2010) Along-strike variations in short-term slow slip events in the southwest Japan subduction zone. J Geophys Res 115:B00A27. https://doi.org/10.1029/2008JB006059

Shelly D, Beroza G, Ide S (2007) Non-volcanic tremor and low-frequency earthquake swarms. Nature 446:305–307. https://doi.org/10.1038/nature05666

Suyehiro S (1979) Continuous observation of crustal movement and borehole strainmeter (I). Weather Serv Bull 46:9–25 (**(in Japanese)**)

Szeliga W, Melbourne T, Santillan M, Miller M (2008) GPS constraints on 34 slow slip events within the Cascadia subduction zone, 1997–2005. J Geophys Res 113:B04404. https://doi.org/10.1029/2007JB004948

Tamura Y, Sato T, Ooe M, Ishiguro M (1991) A procedure for tidal analysis with a Bayesian information criterion. Geophys J Int 104:507–516. https://doi.org/10.1111/j.1365-246X.1991.tb05697.x

Villegas-Lanza JC, Nocquet JM, Rolandone F, Vallée M, Tavera H, Bondoux F, Tran T, Martin X, Chlieh M (2016) A mixed seismic–aseismic stress release episode in the Andean subduction zone. Nat Geosci 9(2):150–154. https://doi.org/10.1038/ngeo2620

Wallace LM, Beavan J (2010) Diverse slow slip behavior at the Hikurangi subduction margin. New Zealand J Geophys Res 115:B12402. https://doi.org/10.1029/2010JB007717

Wech AG, Boese CM, Stern TA, Townend J (2012) Tectonic tremor and deep slow slip on the alpine fault. Geophys Res Lett 39:L10303. https://doi.org/10.1029/2012GL051751

Wessel P, Smith WHF, Scharroo R, Luis J, Wobbe F (2013) Generic mapping tools: improved version released. EOS Trans Am Geophys Union 94(45):409. https://doi.org/10.1002/2013EO450001

Yabe S, Ide S (2018) Variations in precursory slip behavior resulting from frictional heterogeneity. Prog Earth Planet Sci 5:43. https://doi.org/10.1186/s40645-018-0201-x

Yabe S, Ochi T, Itaba S, Matsumoto N, Kitagawa Y, Kiguchi T, Kimura H, Kimura T, Matsuzawa T, Shiomi K (2020a) Short-term slow slip events in the Tokai area, the Kii Peninsula and the Shikoku district, Japan (from may 2019 to october 2019. Rep Coord Comm Earthq Predict 103:166–180

Yabe S, Ochi T, Itaba S, Matsumoto N, Kitagawa Y, Kiguchi T, Kimura H, Kimura T, Matsuzawa T, Shiomi K (2020b) Short-term slow slip events in the Tokai area, the Kii Peninsula and the Shikoku district, Japan (from november 2019 to april 2020). Rep Coord Comm Earthq Predict 104:216–264

Yabe S, Ochi T, Itaba S, Matsumoto N, Kitagawa Y, Kiguchi T, Kimura H, Kimura T, Matsuzawa T, Shiomi K (2021a) Short-term slow slip events in the Tokai area, the Kii Peninsula and the Shikoku district, Japan (from may 2020 to october 2020). Rep Coord Comm Earthq Predict 105:214–258

Yabe S, Och T, Itaba S, Matsumoto N, Kitagawa Y, Kiguchi T, Kimura H, Kimura T, Matsuzawa T, Shiomi K (2021b) Short-term slow slip events in the Tokai area, the Kii Peninsula and the Shikoku district, Japan (from november 2020 to april 2021). Rep Coord Comm Earthq Predict 106:271–322

Yokota Y, Ishikawa T, Watanabe S, Tashiro T, Asada A (2016) Seafloor geodetic constraints on interplate coupling of the Nankai trough megathrust zone. Nature 534(7607):374–377. https://doi.org/10.1038/nature17632

Yoshioka S, Matsuoka Y (2013) Interplate coupling along the Nankai trough, southwest Japan, inferred from inversion analyses of GPS data: effects of subducting plate geometry and spacing of hypothetical ocean-bottom GPS stations. Tectonophysics 600:165–174. https://doi.org/10.1016/j.tecto.2013.01.023

Publisher's Note